2018-03-15

Synthesis and Thermodynamics of Tapered Optical Nanofibers

Anderson, Paul

UNIVERSITY OF CALGARY

Synthesis and Thermodynamics of Tapered Optical Nanofibers

by

Paul Anderson

A THESIS

SUBMITTED TO THE FACULTY OF GRADUATE STUDIES

IN PARTIAL FULFILLMENT OF THE REQUIREMENTS FOR THE

DEGREE OF MASTER OF SCIENCE

GRADUATE PROGRAM IN PHYSICS AND ASTRONOMY

CALGARY, ALBERTA

MARCH, 2018

Abstract

This thesis pertains to the synthesis and use of tapered nanofibers (TNF) in quantum optics experiments. TNFs are optical fibers which contain a region radially tapering down to a submicron diameter. The key feature of such fibers is that a significant portion of an internally propagating electromagnetic field is just outside the fiber in the form of an evanescent field. TNFs are used to substantially improve light-matter interactions by providing a constant small focus of light along millimeters or centimeters of length. Here we report the successful synthesis of a low-loss TNF of custom geometry both theoretically and experimentally. Additionally, we study the thermodynamics of such fibers, demonstrating the ability to measure their temperature resulting from a coupled laser. Finally, we demonstrate the ability to recover lost transmission, due to atoms adsorbed on the fiber's surface. We conclude with an outlook on future experiments with TNFs.

Acknowledgements

I would like to start by thanking my supervisor Alex Lvovsky for accepting me into his group and providing me with guidance as I pursued this degree. I want to thank my colleagues: Di, Shreyas, Anastasiia and Eugene. They helped me create a good working environment which allowed us to complete not one but two successful experiments. There were points in time when this feat was not envisioned to be achieved in such a short time span.

I wish to express my sincere gratitude to Professor Paul Barclay, whom allowed us to work long hours in his lab fabricating nanofibers for our experiment. Without his acceptance and thoughtful input, our nanofibers would be far from the quality we have obtained presently. I would also like to acknowledge the members of Professor Barclay's group. Their kindness and help while we worked in their lab made nanofiber manufacturing much more enjoyable.

All students and researchers alike go through hardships while striving for their goals; searching to find the truth behind some of the mysteries in the world. I firmly believe that it is not possible to overcome these hardships without the help of fellow researchers. To achieve something great requires peers that both provide you with multiple views and challenge you to find the right answer. While attempting to succeed in my endeavors, I felt that the discussions with my colleagues were what truly enabled us to garner meaningful results.

Last, but certainly not least, I would like to thank my family. My mom and dad Catherine and Brian, my sister Sarah and my grandparents Donna and Bill. These are the people who first inspired my drive to find answers. Without them, I would never be able to have the opportunity to contribute my knowledge and insight like this. For that, I am truly grateful.

Table of Contents

Abstract . . . ii
Acknowledgements . . . iii
Table of Contents . . . iv
List of Tables . . . v
List of Figures . . . vi
List of Symbols . . . viii
1 Introduction . . . 1
2 Solutions for the fields propagating through a step-index fiber . . . 4
2.1 Electromagnetic fields at the waist of a TNF . . . 4
2.2 Propagation constant for a step-index fiber . . . 9
3 Theory of fiber pulling . . . 12
3.1 Design of tapered fibers . . . 12
3.2 Adiabatic Taper design . . . 17
3.3 Algorithmic process . . . 21
4 Experimental implementation of nanofiber pulling . . . 23
4.1 Experimental setup . . . 23
4.2 Experimental procedure . . . 23
4.2.1 Measuring the flame width . . . 23
4.2.2 Pulling preparation . . . 27
4.2.3 Fiber preparation . . . 29
4.2.4 Fiber extraction . . . 30
5 Theory of TNF thermometry . . . 31
5.1 General approach . . . 31
5.2 Fluctuational Electrodynamics (FED) Calculations . . . 32
5.3 Heating Power . . . 35
6 Experimental thermometry of optical nanofibers via double heterodyne detection . . . 37
6.1 Experiment . . . 37
6.2 Rubidium desorption . . . 42
7 Conclusion and outlook . . . 45
Bibliography . . . 47

List of Tables

4.1 List of components used in the fiber pulling setup along with their description or brand. 25

List of Figures and Illustrations

2.1 The surface intensity of a 1 mW 795 nm laser beam, coupled into a TNF, as a function of radius. 8

2.2 Effective refractive indices, of the fundamental HE_{11} (blue line) and first excited HE_{12} (red line) modes, for a TNF as a function of its radius. Around $20\mu m$, one can see that the trend for the fundamental mode begins to change as it connects the propagation behaviour of the unpulled region with the vacuum-clad waist. An enhanced view of the effective refractive indices at large radii is shown for clarity (inset). 11

3.1 The heat from the flame of width L_0 heats a section of the fiber as it is pulled symmetrically by two motors. This section is elongated by an amount $\frac{dx}{2}$ on both sides (a total elongation of dx). Due to the conservation of the volume, an elongation corresponds to a decrease in the radius. 13

3.2 Representation of an arbitrary pulling step. A) The very beginning of the step; the point z_α is the first point on the fiber waist and will be the first point to be fully swept by the flame. The point z_ω is the last point on the waist that will be fully swept by the flame. B) A sufficient time t_0 has passed such that the point z_α has been swept by the flame. The point z_ω has moved to the right due to pulling. 14

3.3 Plot of maximum permitted delineation angle as a function of fiber radius. The region between 12 μm and 28 μm, roughly, is the most critical as an angle below 2 milliradians is required. Outside of this regime, the angle requirement is much more relaxed and can be chosen to suit the needs to the experimenter. 19

3.4 Simulation of a TNF created by our algorithm. The fiber is pulled from a starting radius of 62.5 μm down to 44 μm at a slope of 4 milliradians. We then pull down to a 6 μm radius at a slope of 2 milliradians, after which the final waist radius of 230 nm is achieved exponentially. The length of the waist is 10 mm. We used an effective flame width of 800 μm for this simulation. 22

4.1 Picture of the pulling rig setup (Without the flowbox enclosure). 24

4.2 Diagram of the pulling rig setup. 24

4.3 Design of the torch head. There are 29 holes in a hexagonal pattern, each with a diameter of 180 μm. 27

4.4 Example plot of a flame width measurement, the measured flame width was 826 μm. Each data point is separated by 2 seconds of pulling leading to a total pull time of 32 seconds. We use at least 30 seconds of pulling to ensure that we have a constant effective flame width (dictated by the linearity of the graph). The expected slope of the graph is L_0^{-1}. 28

5.1 Theoretical temperature profile of the fiber at equilibrium. Graph plotted for input optical power of 1 mW and 3 mW. The proportionality constant $k = 0.0306$ for both powers. The position 0 is denoted as the center of the fiber. 36

6.1 Experimental setup. Abbreviations: PBS(Polarized Beam Splitter), FC (Fiber Coupler), BHD (Optical Balanced Heterodyne Detector), AOM (Acousto-Optic Modulator). The nanofiber is housed in a vacuum chamber under ultra-high vacuum ($\leq 10^{-8}$ Torr. 39
6.2 Phase accumulated for heating and cooling cycles for transmitted power of 1 mW (blue) and 3 mW (red). 40
6.3 Phase difference between heating and cooling cycles as a function of heating power.The experimental data(red points) is within the predicted errors(blue) even for low heating powers(inset). The primary source of error is the uncertainty(5%) in the radius profile of the nanofiber. 41
6.4 Surface temperature at the waist of the nanofiber as a function of input power. These temperatures correspond to the phase data displayed in fig. 6.3 for the same input power. 42
6.5 Relative transmission of the fiber and the corresponding surface temperature (purple) as a function of the transmitted heating power (blue). 44

List of Symbols, Abbreviations and Nomenclature

Symbol	Definition
AOM	Acousto-optic modulator
a	Physical radius of fiber
BHD	Balanced heterodyne detector
BS	Beam splitter
c_p	Heat capacity
DAQ	Data Acquisition (equipment)
DLCZ	Duan, Lukin, Cirac and Zoller (protocol)
EH	Hybrid electric (mode)
E_r	Radial component of electric field
E_θ	Angularl component of electric field
E_z	transverse component of electric field
f	Degrees of freedom of N_2
H_{rad}	Heat radiated from the fiber
HE	Hybrid electric (mode)
HE_{11}	Fundamental mode
HE_{12}	First-excited mode inside fiber
H_r	Radial component of magnetic field
H_θ	Angularl component of magnetic field
H_z	transverse component of magnetic field
$I(r)$	Surface intensity of fiber at radius r
IPA	Isopropyl alcohol
$J(x)$	Bessel function of the first kind
$J'(x)$	Derivative of first kind Bessel function with respect to x

k_B	Boltzmann's constant
$K(x)$	Bessel function of the second kind
$K'(x)$	Derivative of second kind Bessel function with respect to x
k_0	Vacuum propagation constant
L_0	Effective flame width
L_n	Travel distance of torch
$L_{w,n}$	Length of the pulled-fiber's waist after the nth step
LIAD	Light-induced atomic desorption
LO	Local oscillator
M	Molecular mass of N_2
MOT	Magneto-optical trap
n_{core}	Refractive index of the fiber's core
n_{cladding}	Refractive index of the fiber's cladding
n_{eff}	Effective refractive index of the fiber
N	Number of steps it takes to exponentially pulla fiber to a specific radius
P_0	Input optical power into fiber
P_{heating}	Power of the heat source
p	Pressure of surrounding N_2
PBS	Polarizing beam splitter
QIP	Quantum information processing
r	Radial axis of fiber
r_n	Radius of pulled=fiber's waist after the nth step
r_0	Original radius of an unpulled fiber
r_w	Radius of the waist of a TNF
^{87}Rb	Rubidium 87
SMF	Single-Mode Fiber

U of C	University of Calgary
T	Temperature
T_0	Room temperature
$T_{l,\xi}^{PP\prime}$	Scattering-amplitude matrix element
TE	Transverse-Electric (mode)
t_h	Heating time for fiber pulling
t_0	Time it takes for a point on a pulled-fiber's waist to be swept by flame
TM	Transverse-Magnetic (mode)
Ti:Sa	Titanium sapphire (laser)
TNF	Tapered (optical)Nanofiber
UV	Ultra-violet
v_b	Speed of torch
v_f	Fiber pulling speed
$v_{f,n}$	Fiber pulling speed in the nth step
XPM	Cross phase modulation
z_α	First point on pulled-fiber's waist that is swept by flame
z_Ω	Last point on the pulled-fiber's waist that is swept by the flame
α_{so}	Strain-optic coefficient of silica
α_{te}	Thermal expansion coefficient of silica
β	Axial phase constant
β_{11}	Propagation constant of the fundamental mode
β_{12}	Propagation constant of the first-excited mode
Δl	Change in the optical path length of a fiber
$\Delta\phi$	Change of phase of light beam passing through TNF
ε_1	Dielectric constant of the fiber's core
ε_2	Dielectric constant of the fiber's cladding

λ	Wavelength of light
λ_c	Heat conductivity
μ_0	Magnetic permeability of vacuum
μ_1	Relative magnetic permeability of the fiber's core
μ_2	Relative magnetic permeability of the fiber's cladding
μ_p	Poisson's ration for silica
ν	Optical frequency
ρ	Density of silica
$\Omega(r)$	Maximum delineation angle for adiabacicity
Ω_n	Angle of linear taper of pulled-fiber after the nth step
ω	Angular frequency of electromagnetic wave

Chapter 1

Introduction

In the advent of quantum computation, significant effort is being placed into the implementation of quantum analogs for key classical computational components. Such components include repeaters, random-access memory and logic gates, among others. These implementations cover an extremely wide range of fields from optics to superconductivity, each with their own advantages and problems. In the field of optics, a critical challenge appears in the lack of interaction between two photons or two beams of light. This topic can arise when concepts like cross-phase modulation, quantum memory and all-optical switches are discussed. To remedy this, a proxy is introduced in order to mediate this interaction. A popular proxy of choice is a cold atomic cloud, specifically alkali atoms like Rubidium or Cesium. The primary reasoning for this is the anharmonicity of atoms; the nonlinearity of atoms can be illustrated by the fact that, after absorbing a photon they are much less likely to absorb another one. The result is a strong nonlinear effect at the single photon level, addressing the complication discovered when attempting to use macroscopic nonlinear crystals. Unfortunately, the use of atoms is not entirely a complete and perfect solution. The execution of cold atomic clouds is not a trivial as having light fields incident with the cloud. Given a light field which is resonant with an atom, the absorption cross section of that atom will be slightly larger than λ^2 with λ being the wavelength of the light field. In general, it is extremely difficult to focus a light beam down to a spot size on the order of its wavelength (the minimum spot size depends on the wavelength in addition to the method used to focus). Even if one manages to get close to this size, the distance at which it persists will be minute. To exemplify, one could take a 780 nm laser and focus it down to a spot size of around 780 nm (assuming it is plausible to do so) the Rayleigh length would be $R_z = \frac{\pi w_o^2}{\lambda} \approx 2.45\mu$m. This severely reduces the interaction "window" for the photon and atom, both temporally and spatially. The spatially limiting factor is the cross-sectional

size of the atom being often quite smaller than the minimum spot size of a laser. The temporally limiting factor is the rate of which a light beam will diverge very quickly if focused to that size. Combined, these factors lead to a difficulty to couple light beams to a cloud of atoms in free space with the hopes of strong interactions. Thus, we need to utilize something which either increases the interaction window temporally or spatially. Fortunately, there exists something for both. One could employ an optical cavity, which consists of two high quality mirrors continuously reflecting the light, containing the light within the cavity [2]. If one places an atomic cloud inside, the cavity would increase the number of chances the light could interact with an atom, effectively increasing the interaction window temporally (generally referred to as increasing the effective cross-sectional area). An alternate approach exploits the spatial properties of field-modes in superficial or volume optical waveguides [3]. Examples of the latter are hollow optical fibers where atoms are placed at the center of the fiber where most of the guided light mode is confined. Strong light confinement also takes place in the evanescent field surrounding optical waveguides. Particularly, one could use a tapered optical nanofiber (TNF). TNFs are simply commercial optical fibers which have been pulled, over a sufficient heat source such as a flame, such that the fiber has a consistent submicron diameter for a substantial length [4]. The key property of TNFs is, due to their small diameter at their waist, a significant portion of light propagating through the fiber will be in the form of an evanescent field just outside the surface [5]. This evanescent field is of a consistent size and focus for the entire length of the TNFs waist. Given that the length of a TNF waist is often millimeters to centimeters, which is much larger than the micron-sized value we obtained from the Rayleigh length for free space. Currently, TNFs are a cost-effective approach to aid in light-matter interaction experiments which can be manufactured consistently in terms of quality and geometry. A major difficulty in their use with atomic clouds is the possible adsorption of the atoms onto the surface of the TNF. This not only decreases the transmission of the TNF but it also weakens the integrity of the fiber, increasing the risk of breakage. This thesis presents a means of desorbing atoms by exploiting the thermodynamics of TNFs By coupling a relatively powerful light beam

into a contaminated fiber, the fiber will partially absorb the light that leads to heating of the surface. Attaining a sufficient surface temperature causes the desorption of any atoms on the fiber which gives rise to a transmission recovery and improves the longevity of the fiber.

The structure of this thesis is as follows. We begin by discussing the theory of light propagating through a TNF, solving equations for the electric and magnetic fields guided both inside and outside of the fiber. Furthering on that, we delve into the theory of pulling TNFs from commercial optic fibers, along with what is needed to achieve a 99% transmission fiber of arbitrary length and diameter. This leads to an examination of the experimental pulling process; including the experimental setup, the equipment used and a detailed procedure on how to successfully and consistently pull and extract a high transmission TNF. Finally, the theory behind the main experiment which examines the thermodynamics of TNFs is reported along with the experimental method and results.

Chapter 2

Solutions for the fields propagating through a step-index fiber

All tapered nanofibers are pulled from single-mode commercial step-index optical fibers (SMF). Step-index fibers are very common; their core and cladding regions have constant refractive indices and their core refractive index is larger than that of the cladding. Such fibers are often what is known as weakly guiding fibers in which the difference between the refractive indices of the core and cladding is minuscule ($n_{\text{core}} - n_{\text{cladding}} \lesssim 0.01$) [6]. These fibers are the focus of this thesis. The study and formulation of the fields propagating through such fibers has been thoroughly done and is reported in many articles and textbooks. Here, we will reproduce some of the solutions and calculations from [6] which are critical to the work presented in the chapters that follow. The goal of this chapter is to establish a knowledge of the fields propagating inside and outside the waist of a TNF, enabling us to better understand how to manufacture high quality TNFs (how to adiabatically pull) and possible thermalization mechanisms (heating via optical power).

2.1 Electromagnetic fields at the waist of a TNF

When solving for the field components from Maxwell's equations, one obtains several solutions. Each of these solutions is ascribed an azimuthal mode number, n, and a propagation or axial phase constant, β [6]. These solutions are categorized into four types or modes: transverse-electric (TE) modes have $E_z = 0$ and $E_r = 0$, transverse-magnetic (TM) modes have $H_z = 0$ or $E_\theta = 0$, and the hybrid modes HE and EH (r, θ, z denote cylindrical coordinates) [6]. The latter two mode types have all nonzero field components, with HE customarily having $E_z > \mu c H_z$ and EH usually has $\mu c H_z > E_z$. For optical fibers, only the hybrid modes can exist beyond $n = 0$ and they are the main modes that we focus on. Moreover, since TNFs are almost exclusively pulled from single mode fibers, the only mode that is of concern is the fundamental, HE_{11}, mode. Note that its

designation as the fundamental mode is more so a convention due to the fact that is it the lowest-order mode [6]. By design, the final diameter of the fiber is chosen such that the only mode that persists through the waist of a TNF is still HE_{11}. As a small aside, the single mode property of an optical fiber is governed by what is colloquially known as the V parameter, defined to be $V = \frac{2\pi}{\lambda} a \sqrt{n_{\text{core}}^2 - n_{\text{cladding}}^2}$. For the fiber waist to only allow the fundamental mode, we must have $V \lesssim 2.405$. Below are the solutions for the cylindrical field components for both core and cladding regions of a fiber of radius a as written in [6].

$$\text{For } r \leq a: \qquad E_z = AJ_1\left(\frac{ur}{a}\right)\sin(\theta) \tag{2.1}$$

$$E_r = \left[-A\frac{i\beta}{u/a}J_1'\left(\frac{ur}{a}\right) + B\frac{i\omega\mu_0}{(u/a)^2}\frac{1}{r}J_1\left(\frac{ur}{a}\right)\right]\sin(\theta) \tag{2.2}$$

$$E_\theta = \left[-A\frac{i\beta}{(u/a)^2}\frac{1}{r}J_1\left(\frac{ur}{a}\right) + B\frac{i\omega\mu_0}{u/a}J_1'\left(\frac{ur}{a}\right)\right]\cos(\theta) \tag{2.3}$$

$$H_z = BJ_1\left(\frac{ur}{a}\right)\cos(\theta) \tag{2.4}$$

$$H_r = \left[A\frac{i\omega\varepsilon_1}{(u/a)^2}\frac{1}{r}J_1\left(\frac{ur}{a}\right) - B\frac{i\beta}{u/a}J_1'\left(\frac{ur}{a}\right)\right]\cos(\theta) \tag{2.5}$$

$$H_\theta = \left[-A\frac{i\omega\varepsilon_1}{u/a}J_1'\left(\frac{ur}{a}\right) + B\frac{i\beta}{(u/a)^2}\frac{1}{r}J_1\left(\frac{ur}{a}\right)\right]\sin(\theta) \tag{2.6}$$

where

$$u = k_0 a\sqrt{n_1^2 - \beta_{11}^2} \tag{2.7}$$

For $r > a$:

$$E_z = CK_1\left(\frac{wr}{a}\right)\sin(\theta) \tag{2.8}$$

$$E_r = \left[C\frac{i\beta}{w/a}K_1'\left(\frac{wr}{a}\right) - D\frac{i\omega\mu_0}{(w/a)^2}\frac{1}{r}K_1\left(\frac{wr}{a}\right)\right]\sin(\theta) \tag{2.9}$$

$$E_\theta = \left[C\frac{i\beta}{(w/a)^2}\frac{1}{r}K_1\left(\frac{wr}{a}\right) - D\frac{i\omega\mu_0}{w/a}K_1'\left(\frac{wr}{a}\right)\right]\cos(\theta) \tag{2.10}$$

$$H_z = DK_1\left(\frac{wr}{a}\right)\cos(\theta) \tag{2.11}$$

$$H_r = \left[-C\frac{i\omega\varepsilon_2}{(w/a)^2}\frac{1}{r}K_1\left(\frac{wr}{a}\right) + D\frac{i\beta}{w/a}K_1'\left(\frac{wr}{a}\right)\right]\cos(\theta) \tag{2.12}$$

$$H_\theta = \left[C\frac{i\omega\varepsilon_2}{w/a}K_1'\left(\frac{wr}{a}\right) - D\frac{i\beta}{(w/a)^2}\frac{1}{r}K_1\left(\frac{wr}{a}\right)\right]\sin(\theta) \tag{2.13}$$

where

$$w = k_0 a\sqrt{\beta_{11}^2 - n_2^2} \tag{2.14}$$

$J(x)$ and $K(x)$ are Bessel functions of the first and second kind, respectively. $J'(x)$ and $K'(x)$ are the derivatives of the Bessel functions with respect to x. k_0 is the vacuum propagation constant, β_{11} the propagation constant for the HE_{11} mode, μ_0 is the magnetic constant, μ_1 and μ_2 are the relative permeability constants for the fiber's core and cladding respectively, ε_1 and ε_2 are the dielectric constants for the fiber's core and cladding, respectively. n_1 and n_2 are the refractive

indices for the core and cladding, respectively.

A, B, C and D are coefficients that are found using several boundary conditions which must be met to obtain physical solutions. These solutions stem from the requirement of continuity of the fields at the core-cladding boundary. Thus, at $r = a$ we must have:

$$E_z^{\text{core}} = E_z^{\text{cladding}} \tag{2.15}$$

$$E_\theta^{\text{core}} = E_\theta^{\text{cladding}} \tag{2.16}$$

$$\varepsilon_1 E_r^{\text{core}} = \varepsilon_2 E_r^{\text{cladding}} \tag{2.17}$$

$$H_z^{\text{core}} = H_z^{\text{cladding}} \tag{2.18}$$

$$H_\theta^{\text{core}} = H_\theta^{\text{cladding}} \tag{2.19}$$

$$\mu_1 H_r^{\text{core}} = \mu_2 H_r^{\text{cladding}} \tag{2.20}$$

Using these conditions in conjunction with the general field equations leads to four equations, of which the four coefficients must satisfy.

$$AJ_1(u) - CK_1(w) = 0 \tag{2.21}$$

$$BJ_1(u) - DK_1(w) = 0 \tag{2.22}$$

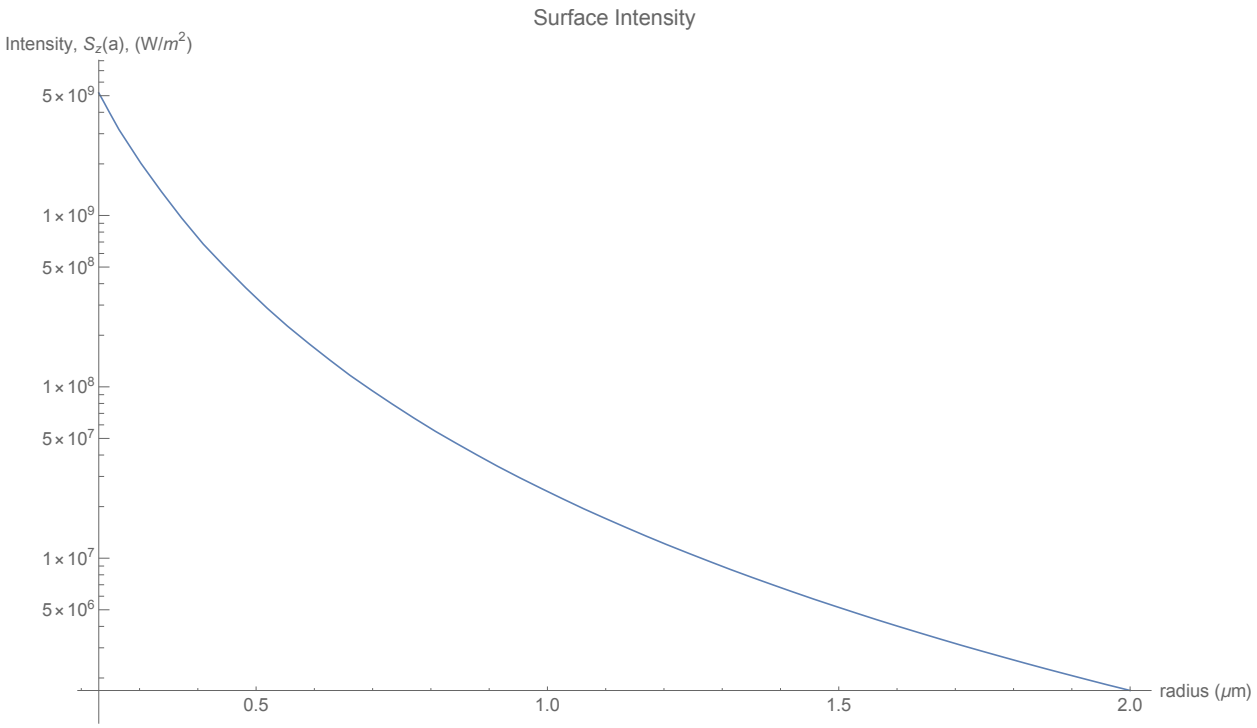

Figure 2.1: The surface intensity of a 1 mW 795 nm laser beam, coupled into a TNF, as a function of radius.

$$A\frac{i\beta}{(u/a)^2}\frac{J_1(u)}{a} - B\frac{i\omega\mu_0}{u/a}J_1'(u) + C\frac{i\beta}{(w/a)^2}\frac{K_1(w)}{a} - D\frac{i\omega\mu_0}{w/a}K_1'(w) = 0 \tag{2.23}$$

$$A\frac{i\omega\varepsilon_1}{u/a}J_1'(u) - B\frac{i\beta}{(u/a)^2}\frac{J_1(u)}{a} + C\frac{i\omega\varepsilon_2}{w/a}K_1'(w) - D\frac{i\beta}{(w/a)^2}\frac{K_1(w)}{a} = 0 \tag{2.24}$$

Before finding these coefficients, the only remaining unknown parameter needed to obtain the electromagnetic fields is the propagation constant, β. Although the field components themselves are not terribly beneficial on their own, we can use them to ascertain values which can directly tell us how the TNFs can be utilized. For example, one such value is the electric intensity $|E|^2$ which is proportional to the trapping intensity; this is used to characterize the trapping of atoms by optical force [7]. Of course, even if one were to calculate the needed intensity for atom trapping, the TNF

propagating this field must be able to withstand the optical power of the laser. Thus, another useful parameter to calculate is the surface intensity. This parameter helps us understand how a fiber is heated by an optical field and is characterized by the Poynting vector magnitude $S(r)$. Figure 2.1 shows the Poynting vector magnitude at the fiber surface for different radii. One can see that as the fiber radius increases, the surface intensity decreases exponentially. To better illustrate this, at 10 μm in radius, the surface intensity will be more than 1 million times smaller than at the waist radius of 230 nm. This tells us that most of the intensity occurs at the waist and a small portion of the taper beyond it. This can be quite useful as it helps in understanding the underlying mechanism of optically heating a fiber.

2.2 Propagation constant for a step-index fiber

The propagation constant is a needed parameter when examining the fields and mode solutions for these fibers. Additionally, it also proves to be extremely useful when assessing the adiabaticity of TNF manufacturing (discussed in chapter 3). We can create an equation for β by combining the four equations (2.21)-(2.24) which results in

$$\left[\frac{J_1'(u)}{uJ_1(u)}+\frac{K_1'(w)}{wK_1(w)}\right]\left[\frac{\varepsilon_1 J_1'(u)}{\varepsilon_2 uJ_1(u)}+\frac{K_1'(w)}{wK_1(w)}\right]=\left[\frac{1}{u^2}+\frac{1}{w^2}\right]\left[\frac{\varepsilon_1}{\varepsilon_2 u^2}+\frac{1}{w^2}\right] \tag{2.25}$$

If one writes both u and w in terms of β then one can solve for β. Since the above is a transcendental equation, it can produce multiple solutions when solved numerically. Since we require $u, w \in \mathbb{R}$, we must impose a constraint on the possible values of β [6]. We have $u, w \in \mathbb{R}$ when β falls in the range

$$n_{\text{cladding}} k_0 < \beta < n_{\text{core}} k_0 \tag{2.26}$$

Eq. (2.26) allows us to obtain the correct value of β when solving eq. (2.25). This method for ascertaining the propagation constant, known as the two-layer model, is sufficient for most applications regarding TNFs as most of the time we are only concerned with the waist (one can

refer back to the discussion of the small surface intensity beyond the waist). At the waist, what was once the fiber's core is now so minuscule that the coupled light will simply propagate via the cladding. The environment outside the TNF (often vacuum or air) will then act as the cladding. This is sometimes called vacuum-clad and it is important to note that, here, the weakly-guided approximation will no longer hold. You must solve (2.25) as is without simplifications. However, complications begin to arise when we want to analyze the properties on the taper, specifically in the region between $20\mu m$ and $45\mu m$, in radius. In this regime, the cladding is still large, but not large enough to prevent the outside environment from playing a role. For this, we must employ a three-layer model. Fortunately, work has been previously done on this, and a program exists to calculate the propagation constant for TNFs [8]. Figure 2.2 depicts the effective refractive indices for the fundamental and first excited modes in a TNF. The effective refractive index for any mode is related to its propagation constant simply by $\beta = k_0 n_{eff}$, where $k_0 = \frac{2\pi}{\lambda}$. One can see that, for the fundamental mode, there is a difference in behaviour for the propagation at the waist compared to the unpulled region. This is due to the difference in the ratio of the refractive indices for the core and cladding. For the unpulled region, the cladding is silica with a refractive index around 1.45 (Compared to $n_{\text{core}} = 1.455$). However, for the waist, the cladding is the environment of which the refractive index is very close to, or exactly, 1. This leads to the different trends in these regions, but in between, we must still have continuity. Thus, we need to use a three-layer model to connect these regimes smoothly. Knowing the full trend of the propagation constants for all sections of the TNF enables to study the adiabaticity, as we do in chapter 3. Thankfully, as was stated above, if one is only concerned with the physics of the waist then one can simply use the two-layer approach without much need to over-complicate things.

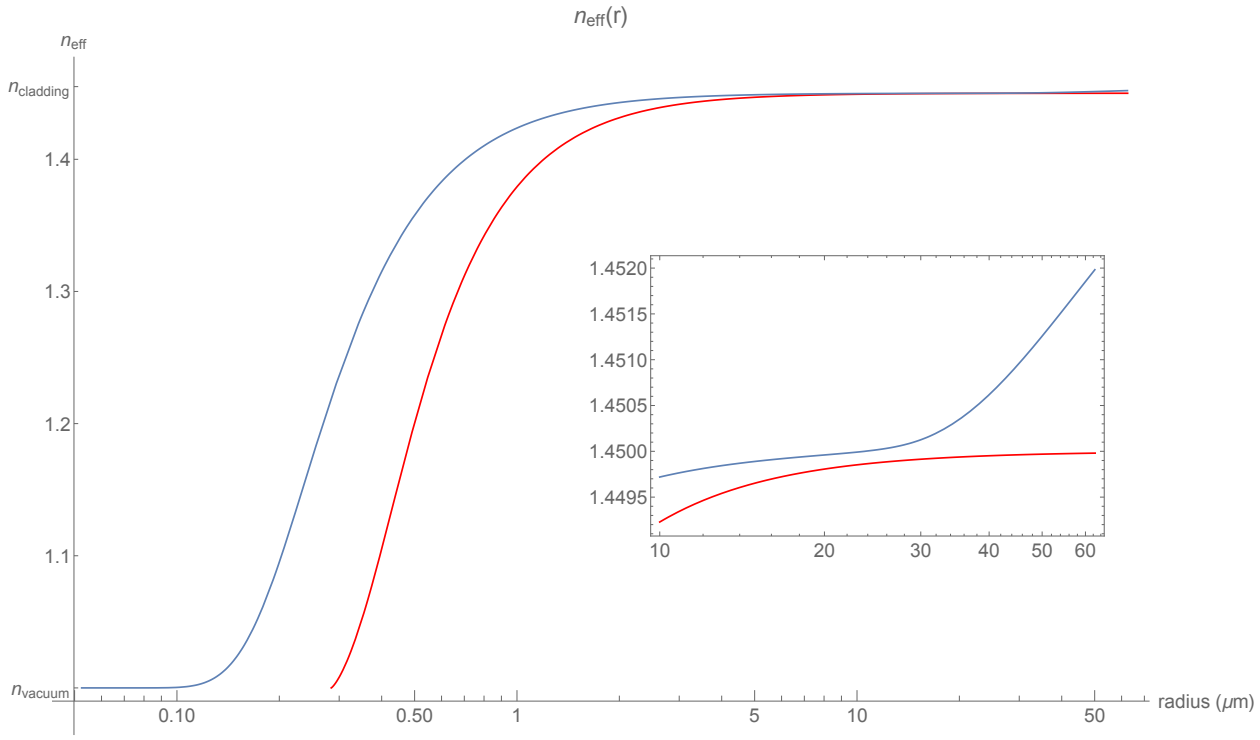

Figure 2.2: Effective refractive indices, of the fundamental HE_{11} (blue line) and first excited HE_{12} (red line) modes, for a TNF as a function of its radius. Around $20\mu m$, one can see that the trend for the fundamental mode begins to change as it connects the propagation behaviour of the unpulled region with the vacuum-clad waist. An enhanced view of the effective refractive indices at large radii is shown for clarity (inset).

Chapter 3

Theory of fiber pulling

3.1 Design of tapered fibers

When manufacturing TNFs for quantum optics experiments it is important to have a methodical approach which has two properties. Firstly, it is desirable to have a method that allows us to customize the geometry of the TNF; this includes the length and diameter of the waist, as well as overall length of the fiber. Secondly, we need the method to be able to consistently produce TNFs, of a particular geometry, which have a transmission loss of 1% or less. To achieve this, we look to the work of Birks *et al.* who designed a theoretical model for stretching a cylinder such that it tapers down to a waist of predetermined diameter for some predetermined length [9]. The bulk of this chapter is following the Ph.D. thesis of Christian Wuttke who wrote the original algorithm for fiber pulling [10]. However, due to the complexity of this theory, there were mistakes present and some parts of it were difficult to interpret. Since we sought to develop a program to pull fibers based on this theory, we first had to decipher it and fix any mistakes. Thus, we shall report a reformatted version of this theory in the hopes that readers will be able to easily understand the concepts and possibly develop their own fibers from it.

The setup of the pulling is as follows. The fiber is attached to two motorized stages which will move apart from each other at the same speed. In between these two stages is a torch which produces a flame of constant width denoted as L_o. Let us analyze the setting in which the torch is stationary. The part of the fiber that is inside the flame is a cylinder of radius r and volume $V = \pi r^2 L_0$. Let us suppose that the motors now stretch this cylinder by some infinitesimal amount dx (see fig. 3.1). We can describe the change of the shape of the cylinder by the following differential equation

$$dV = \pi dx r^2 + 2\pi L_0 r dr \tag{3.1}$$

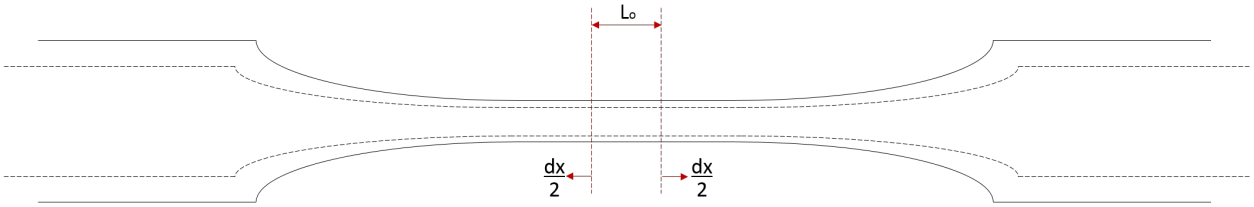

Figure 3.1: The heat from the flame of width L_0 heats a section of the fiber as it is pulled symmetrically by two motors. This section is elongated by an amount $\frac{dx}{2}$ on both sides (a total elongation of dx). Due to the conservation of the volume, an elongation corresponds to a decrease in the radius.

We assume that the volume of the portion inside the flame remains constant throughout the stretching. Thus, the change in volume of the heated portion during pulling will be zero. We can now utilize this to find the change of radius with respect to the elongation amount, x.

$$\begin{aligned} dV &= \pi dx r^2 + 2\pi L_0 r dr = 0 \\ \implies \frac{dr}{dx} &= -\frac{r}{2L_0} \end{aligned} \tag{3.2}$$

and proceed to solve for r as a function of x

$$r(x) = r_0 e^{-\frac{x}{2L_0}} \tag{3.3}$$

Eq. (3.3) tells us how the radius at the center of the cylinder evolves due to an elongation of amount x. The fiber pulling speed, v_f, is defined as the relative speed of both motors, if both motors move at $\frac{v_f}{2}$. If the time of the step is defined as t_h, then the fiber will be pulled by an amount $x = v_f t_h$. The final radius attained is r_f

$$r_f = r_i e^{-\frac{t_h v_f}{2L_0}} \tag{3.4}$$

where r_i is the initial radius before pulling.

From here, one could simply use eq. (3.3) and obtain a TNF of an appropriate diameter (appropriate meaning a diameter small enough to only support the fundamental mode). However, one would have very little control over other geometrical parameters, namely the length of the waist. With a stationary torch, the fiber waist, defined to be the region which is of a consistent diameter (the

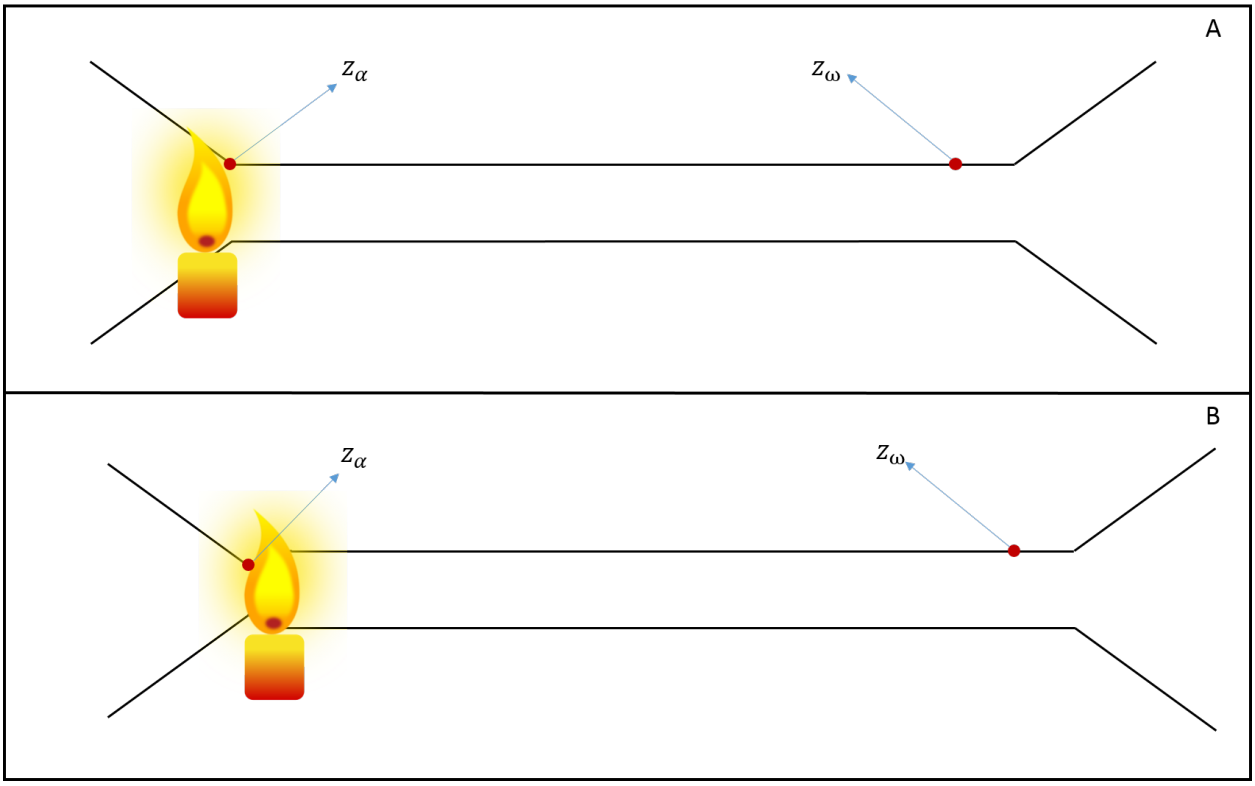

Figure 3.2: Representation of an arbitrary pulling step. A) The very beginning of the step; the point z_α is the first point on the fiber waist and will be the first point to be fully swept by the flame. The point z_ω is the last point on the waist that will be fully swept by the flame. B) A sufficient time t_0 has passed such that the point z_α has been swept by the flame. The point z_ω has moved to the right due to pulling.

smallest diameter reached), would be too short to be useful (1mm) as it is upper-bounded by the flame width. Thus, we must circumvent this by moving the torch at some speed v_b in addition to the movement of the fiber. This means that the torch will sweep across the fiber back and forth while the fiber is being pulled apart. This technique (known as the flame-brush technique [11]).

To characterize and algorithmically manufacture TNFs of specific geometries, we will think of each sweep of the fiber by the flame as a discrete step labeled with some integer n. For every nth step, we will be examining three important parameters: the radius of the waist r_n, the length of the waist $L_{w,n}$ and the total distance traveled by the torch L_n. We begin by looking at the evolution of the radius due to heating. As depicted in fig. 3.2, as the flame sweeps across the waist, the thick portion of the fiber will be thinned and stretched. Let us suppose the fiber is being pulled by two motors both traveling at a speed $\frac{v_{f,n}}{2}$ away from each other while the torch is moving to the right at a speed v_b. In the torch's frame of reference, the section of fiber to the right of the flame will be moving at a relative speed of $v_b - \frac{v_{f,n}}{2}$ whereas the left part will be moving at a relative speed $v_b + \frac{v_{f,n}}{2}$. If some arbitrary time Δt during the nth step the length of the pulled section (on the left of the flame) is denoted as Δl_n and the length of unpulled section is Δl_{n-1} then Δl_n will be increased by an amount $\left(v_b + \frac{v_{f,n}}{2}\right)\Delta t$ and Δl_{n-1} will be decreased by $\left(v_b - \frac{v_{f,n}}{2}\right)\Delta t$. Therefore, the ratio of these lengths will be

$$\begin{aligned} \frac{\Delta l_n}{\Delta l_{n-1}} &= \frac{v_b + \frac{v_{f,n}}{2}}{v_b - \frac{v_{f,n}}{2}} \\ &= \frac{2v_b + v_{f,n}}{2v_b - v_{f,n}} \end{aligned} \tag{3.5}$$

Now, given that the volume of the fiber is conserved as it is pulled we can write this as a ratio of radii.

$$\frac{r_n}{r_{n-1}} = \sqrt{\frac{l_{n-1}}{l_n}} = \sqrt{\frac{2v_b - v_{f,n}}{2v_b + v_{f,n}}} \tag{3.6}$$

Therefore, the evolution of the radius from step $n-1$ to n is

$$r_n = r_{n-1}\sqrt{\frac{2v_b - v_{f,n}}{2v_b + v_{f,n}}} \tag{3.7}$$

In order for the flame to overtake all moving points of the fiber, we must have

$$v_b > \frac{v_f}{2} \tag{3.8}$$

Understanding how the radius evolves at the waist of the fiber is crucial to being able to pull a TNF with a desired final radius, however it is not the only parameter we wish to control. A secondary parameter which we wish to customize is the length of the waist. For any arbitrary step, n, the waist is defined to encompass all points on the fiber which are fully swept by the flame (i.e. points that begin somewhere ahead of the flame and end somewhere behind it). The length of the waist achieved in the nth step is taken to be the distance that these points span at the end of the step. Suppose we call the coordinate of the point, on the fiber, starting at the front edge of the flame at time t $z_\alpha(t)$ and the point ending on the back edge of the flame at time t, $z_\omega(t)$. Let us now look at the step from the perspective of the flame. Let us now suppose that some time has passed such that $z_\alpha(t)$ is now at the back edge of the flame; we will call this time t_0. This means that $z_\alpha(t_0)$ has traversed a distance of L_0. During this time, $z_\omega(t_0)$ will have moved a distance $\left(v_b - \frac{1}{2}v_{f,n}\right)t_0$. If, at the beginning of the step, we have $z_\alpha(0) = 0$ then their displacement after a time t_0 will be

$$z_\alpha(t_0) = -L_0 \tag{3.9}$$

At the end of the step, we want to have $z_\omega(t_n) = -L_0$ (with respect to the front edge of the flame) so that we have $z_\omega(t_n)$ being the last point to be fully swept by the flame. Thus, at the end of the step we have

$$z_\alpha(t_n) = -L_0 - \left(v_b + \frac{1}{2}v_{f,n}\right)(t_n - t_0) \tag{3.10}$$

and

$$z_\omega(t_n) = -L_0 \tag{3.11}$$

where t_n is defined to be the total time it takes for the step to complete.

We defined the length of the waist $L_{w,n}$ to be the final separation between $z_\alpha(t_n)$ and $z_\omega(t_n)$. Since

we know that the flame must travel a distance L_n at a speed v_b, we know that the time to complete the step is $t_n = \frac{L_n}{v_b}$. Thus, we have

$$\begin{aligned} L_{w,n} &= z_\omega(t_n) - z_\alpha(t_n) = \left(v_b + \frac{1}{2}v_{f,n}\right)(t_n - t_0) \\ &= \left(1 + \frac{v_{f,n}}{2v_b}\right)L_n - \left(v_b + \frac{1}{2}v_{f,n}\right)t_0 \end{aligned} \tag{3.12}$$

Our end goal is to be able to pull a TNF with a specific final radius and waist length. Therefore, we wish to have these values as input parameters to our algorithm. Thus, we are interested in calculating the requisite travel distance for the nth step L_n which will achieve a certain waist length $L_{w,n}$. We can rearrange eq. (3.12) to find that

$$L_n = \frac{L_{w,n} + \left(v_b + \frac{1}{2}v_{f,n}\right)t_0}{1 + \frac{v_{f,n}}{2v_b}} \tag{3.13}$$

The one term which we have yet to fully define is t_0. To find the value of this in terms of known parameters, we again look at the nth step from the perspective of the flame. We know that a point which is fully swept by the flame will travel a distance L_0. We assume that, within the flame, points on the fiber which are to the right of the flame's center will move right and points to the left side will move left. Therefore, if we examine a point entering the flame starting on the rightmost edge, we will see it moving left towards the flame's center at a speed $\left(v_b - \frac{1}{2}v_{f,n}\right)$. Once it passes the center of the flame, it will continue to move left but at a speed $\left(v_b + \frac{1}{2}v_{f,n}\right)$. The time it takes to span the width of the flame will be equivalent to it traveling L_0 with an average speed of v_b. Thus, we have

$$t_0 = \frac{L_0}{v_b} \tag{3.14}$$

3.2 Adiabatic Taper design

It is entirely possible to pull a TNF that has a purely exponential taper (i.e. pulled using a stationary flame). However, this method does not permit the customization of the waist length. One can see that, for a stationary flame, the length of the waist is upper-bounded by the effective flame width.

Since physically changing the flame width is not really that feasible, our solution is to move the flame. The second drawback of a pure exponential taper is the lack of control over the slope. TNFs are pulled with a commercial single-mode optical fibers which have a specific geometry which restricts the mode of the propagating light to the HE_{11}. As the fiber is pulled, the original geometry is changed which could allow the existence of higher-order modes of light. Moving the flame not only allows control over the waist length but it also allows the formation of linear tapers. These tapers enables us to slowly decrease the radius; this adiabatic evolution maintains the single-mode criteria and reduces the resulting transmission loss. Of course, a question which will now arise is, what angles allow you to pull an adiabatic taper. For a TNF to be adiabatic we must have a shallow enough angle of declination, such that there is almost no coupling of power to higher-order modes [12]. Mathematically, this is represented as:

$$\Omega(r) = \frac{r}{2\pi}\left(\beta_{11}(r) - \beta_{12}(r)\right) \tag{3.15}$$

$\Omega(r)$ represents the maximum allowed delineation angle for a given radius. $\beta_{11}(r)$ and $\beta_{12}(r)$ are the propagation constants for the fundamental and the first excited modes, respectively. This relation tells us the angle at which there will be no coupling of power to the first excited mode HE_{12}, and therefore no coupling to other excited modes. Eq. (3.15) is plotted in figure 3.3 and shows that, for radii between 12 μm and 28 μm, we must pull at a slope $\lesssim 2$ milliradians. Beyond this, we simply choose a slope which sufficiently shortens the total length to a feasible amount, but still maintains adiabaticity. We also need a relation that tells us what fiber speed is needed to attain a desired angle. For this, let us look at the tapered part of the fiber that is within the flame at the beginning of the nth step. The radius of the fiber of the point immediately at the back edge of the flame will be $r = r_{n-2}$. This is due to the fact that the flame began on the opposite end of the fiber during the $n-1$ step. The point immediately at the front of the flame will be at $r = r_{n-1}$ as it is the last point on the waist created in the previous step. As the flame begins to move during the nth step, the point behind the flame at $r = r_{n-2}$ will not be pulled and will simply move backwards at a speed $v_b + \frac{v_{f,n}}{2}$ relative to the torch. The point in front of the flame will be pulled to $r_{n-1} \to r_n$

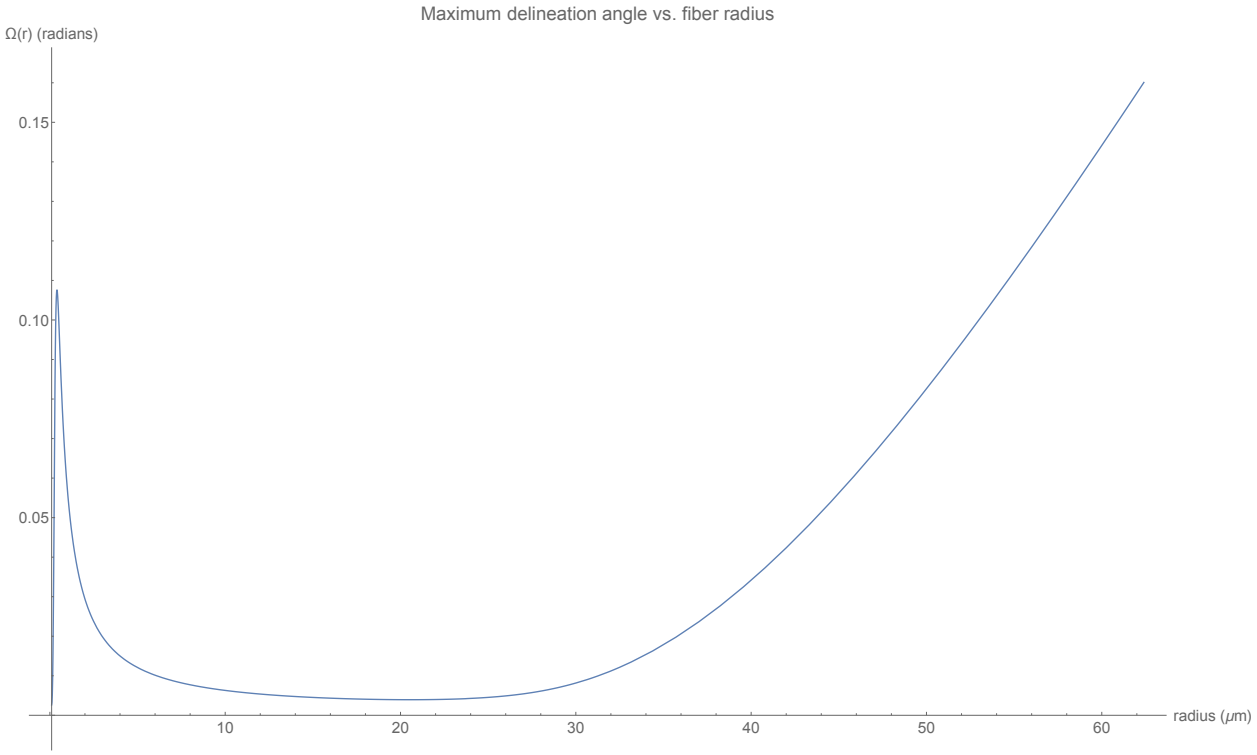

Figure 3.3: Plot of maximum permitted delineation angle as a function of fiber radius. The region between 12 μm and 28 μm, roughly, is the most critical as an angle below 2 milliradians is required. Outside of this regime, the angle requirement is much more relaxed and can be chosen to suit the needs to the experimenter.

and become the first point on the new waist; this evolution will occur after a time t_0. At this time, the point at $r = r_{n-2}$ will have moved a distance $\left(v_b + \frac{v_{f,n}}{2}\right) t_0$. Therefore, we can write the angle of this slope as the following,

$$\begin{aligned} \Omega_n &= \tan^{-1}\left(\frac{r_{n-2} - r_n}{\left(v_b + \frac{1}{2}v_{f,n}\right) t_0}\right) \\ &\approx \left(\frac{r_{n-2} - r_n}{\left(v_b + \frac{1}{2}v_{f,n}\right) t_0}\right) \end{aligned} \tag{3.16}$$

Since we wish to pull adiabatically, we are assuming the angle will always be small enough to use the small-angle approximation. Now we will use eq. (3.7) to write eq. (3.16) in terms of r_n only:

$$\Omega_n \approx \left[\frac{\left(\sqrt{\frac{2v_b+v_{f,n}}{2v_b-v_{f,n}}}\sqrt{\frac{2v_b+v_{f,n-1}}{2v_b-v_{f,n-1}}}\right) r_n}{\left(v_b + \frac{1}{2}v_{f,n}\right) t_0}\right] \tag{3.17}$$

Similarly, we will assume that the radius evolution from step-to-step is very small which allows us to write the above only in terms of nth step parameters. This gives us

$$\Omega_n \approx \left[\frac{\left(\frac{2v_b+v_{f,n}}{2v_b-v_{f,n}}\right) r_n}{\left(v_b + \frac{1}{2}v_{f,n}\right) t_0}\right] \tag{3.18}$$

Since the angle is something we would also like to control as an input parameter for our algorithm, we will rearrange eq. (3.18) and solve for $v_{f,n}$ which enables us to calculate at what speed will generate the desired angle at a particular radius r_n. Expanding eq. (3.18) leads to a quadratic equation in $v_{f,n}$; the solution of it is as follows

$$v_{f,n} \approx \frac{-2r_n \pm 2\sqrt{r_n^2 - \Omega_n^2 t_0^2 v_b^2}}{\Omega_n t_0} \tag{3.19}$$

For this system, negative solutions do not make much physical sense so we choose the positive solution as it is the only viable solution. From eq. (3.19) we see that $v_{f,n}$ remains quite small compared to v_b, often becoming no larger than $\frac{v_b}{4}$. Thus, we can make one additional simplification.

The relation obtained by (3.18) can be written as

$$\Omega_n L_0 \frac{v_{f,n}^2}{v_b^2} + 4r_n \frac{v_{f,n}}{v_b} - 4\Omega_n L_0 \approx 0 \tag{3.20}$$

Neglecting the higher order term of $\frac{v_{f,n}^2}{v_b^2}$ allows us to write $v_{f,n}$ simply as

$$v_{f,n} \approx v_b \frac{\Omega_n L_0}{r_n} \tag{3.21}$$

3.3 Algorithmic process

Finally, we shall utilize the previously derived relations and present the overall procedure of the algorithm. We wish to have an algorithm which accepts: the waist radius and length, the starting radius, the flame width as well as the angles and ending radii of any linear transitions as input parameters. The output are the calculated fiber speeds and the time for each step. The fibers simulated by our algorithm must have at least one linear and one exponential transition. The exponential transition will always be the final transition before the waist. For reasons stated above, we always wish to have at least one linear transition so we believe this constraint to our algorithm is not too constricting. Secondly, all fibers must end exponentially in order to create the radially-constant waist. We need these characteristics in order to begin the calculations in our algorithm. This is due to the requirement of calculating the first set of parameters using only the input values (r_0, r_w, l_w, Ω, etc.). We accomplish this by utilizing a boundary condition which is the matching of slopes between the exponential and the adjacent linear transition. To do this, we use (3.19) to obtain the speed needed at the step just before the exponential begins, using the radius accepted as an input (the radius at which the final linear section ends). This speed is then used as the speed for the entirety of the exponential section (exponential tapers are created when v_f is constant). We,

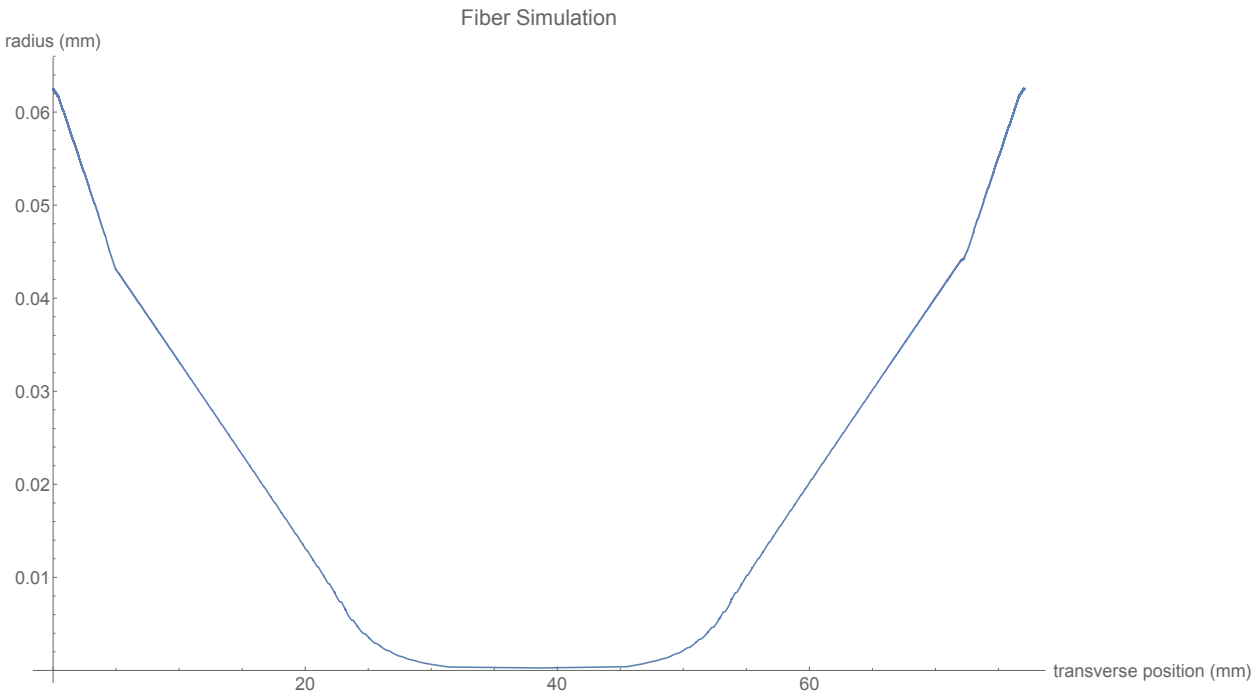

Figure 3.4: Simulation of a TNF created by our algorithm. The fiber is pulled from a starting radius of 62.5 μm down to 44 μm at a slope of 4 milliradians. We then pull down to a 6 μm radius at a slope of 2 milliradians, after which the final waist radius of 230 nm is achieved exponentially. The length of the waist is 10 mm. We used an effective flame width of 800 μm for this simulation.

then, calculate the number of steps for the exponential section using (3.7).

$$\begin{aligned} r_w = r_N &= r_0 \left(\sqrt{\frac{2v_b - v_f}{2v_b + v_f}} \right)^N \\ \implies N &= \frac{2\log\left(\frac{r_w}{r_0}\right)}{\log\left(\frac{2v_b - v_f}{2v_b + v_f}\right)} \end{aligned} \tag{3.22}$$

r_0 is the ending radius of the final linear transition, r_w is the desired waist radius and N is the resultant number of steps needed to complete the exponential section. Finally, we calculate the distance traveled by the torch, L_n, and the step times, t_n, using the appropriate equations. Calculating the parameters for a linear section is quite similar, except the fiber speeds are found using (3.21) before calculating L_n and t_n. All of this is done recursively, starting with the final radius and waist length and parameters are calculated until the original fiber radius is reached. The required parameters for every step are outputted in a text file which is then read and executed by our pulling rig. An example of a fiber profile generated by our algorithm is shown in figure 3.4.

Chapter 4

Experimental implementation of nanofiber pulling

4.1 Experimental setup

To create a tapered nanofiber, we utilize a stainless steel torch with a hydro-oxygen flame along with two fiber clamps on motorized stages (See figures 4.1 and 4.2). The torch is attached to a multi-axis translation stage which is also on a motorized stage. These stages are connected to a computer which controls the velocity and duration of movement of the stages. We use high purity oxygen and hydrogen, regulated by high-accuracy flow meters to generate the flame. During a pull, the fiber is monitored in two ways. First, we use a microscope with a high-power objective attached to a camera to observe the pulling in progress. Second, we send 1-2 mW of 780nm laser through the fiber and into an IR nanosecond photodetector. This allows us to observe the transmission of the fiber while it is being pulled. Refer to table 4.1 for a detailed list of all parts and components for our fiber pulling setup. Finally, since the largest problem encountered when pulling fibers is dust particles settling during and after pulling [13], we encase the entire pulling rig inside an enclosure with polyvinyl strip curtains. Attached to the top of the enclosure is a flowbox which constantly creates a laminar flow of air pushing downwards. This creates a clean environment in which to pull.

4.2 Experimental procedure

4.2.1 Measuring the flame width

Before any pulling begins, we must perform several preparation steps to ensure the best possible outcome. The very first thing we must do before pulling is to measure the effective flame width, L_o. This step has to be done if we are beginning a pulling session after not pulling for a long length of

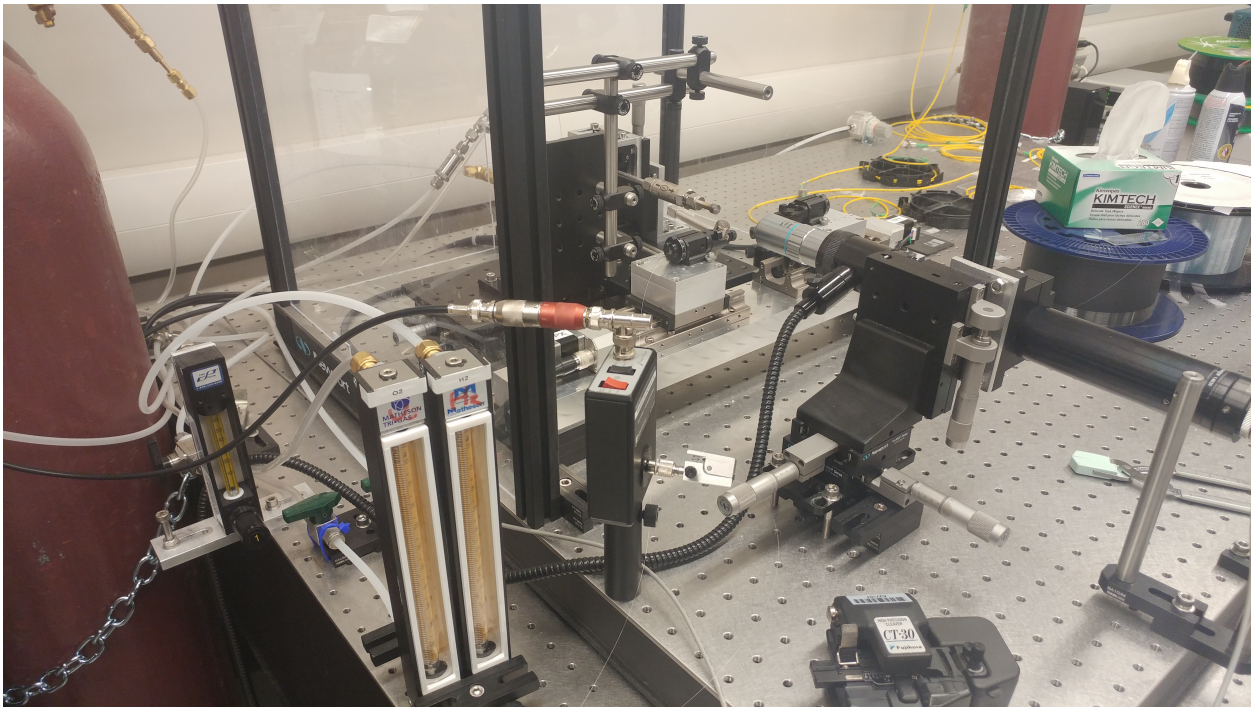

Figure 4.1: Picture of the pulling rig setup (Without the flowbox enclosure).

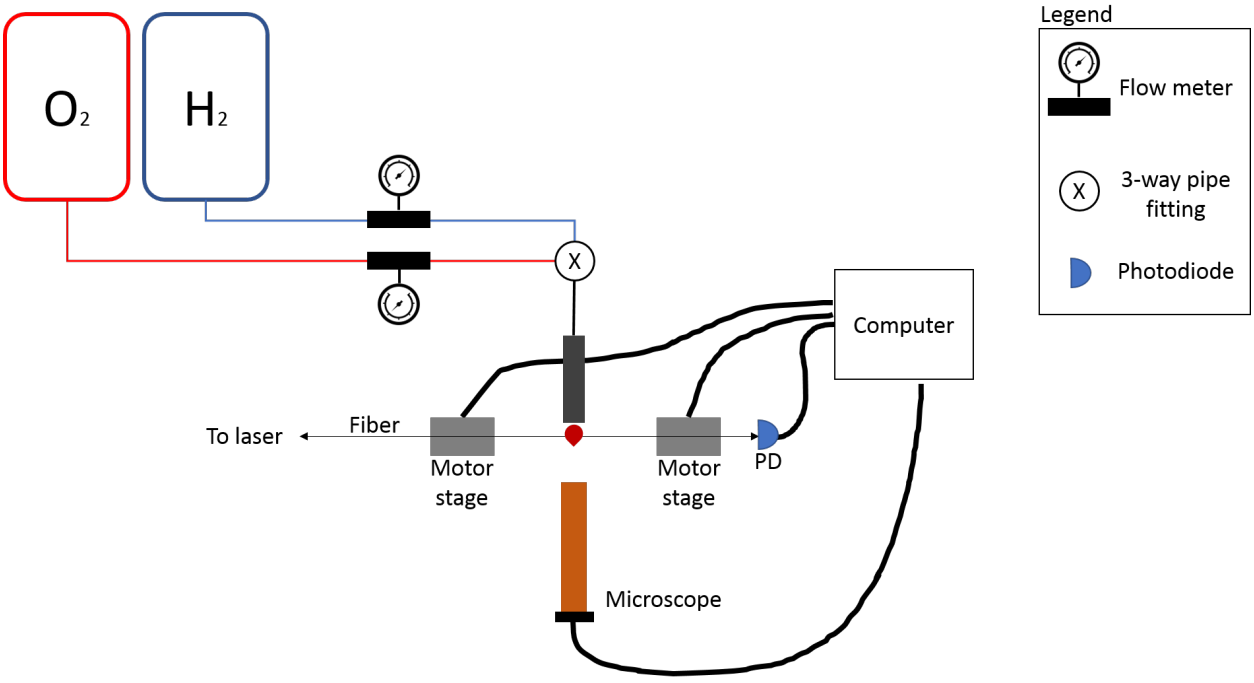

Figure 4.2: Diagram of the pulling rig setup.

Item	**Description**
Three computer-controlled stepping motors	Suruga KXL06050-C1-C
Stepping motor controller	Suruga DS102MS
Two rotating fiber clamps from Thorlabs	Model number HFR007 (fix the bare fiber onto motorized stages)
Hydrogen gas cylinder	Praxair Purity 4.5
Oxygen gas cylinder	Praxair Purity 5.0, cylinder fill pressure 2200 psig, gas volume 6.90m^3, Part number OX 5.0RS-K
National gas regulator	maximum outlet pressure 60 psi
Volume-based gas flow meters	Chrysalis Model FM-1050
Visible photodetector from	New Focus Model number 1621 (to monitor fiber transmission)
UV glue	Dymax OP-4-20632
UV curing lamp	Dymax Bluewave 75 UV Curing Spot Lamp
Fiber cleaver	Ericsson Model number EFC 11
Fiber fusion splicer	Ericsson FSU 995 FA
Swagelok SS-4F-7	Particulate filter, 7μm pore size
GLFPF3000SM4	"Mini Gaskleen filter" from PALL
Custom SS nozzle	29, 200μm holes in a 1x2mm^2 array

Table 4.1: List of components used in the fiber pulling setup along with their description or brand.

time. If we are pulling after having pulled recently then this is not necessary as our torch produces a fairly consistent flame. Ideally, we could use any flame width and the only additional step being the calculation of the pulling speeds (discussed later) using the measured flame width. However, due to possible experimental limitations, we aim to have a flame width somewhere between 600 μm to 900 μm. Ultimately, our flame widths are determined by the shape of the torch head and flow rates of our gases. The design of our torch can be found in fig. 4.3, its holes are in a hexagonal pattern which is approximately 2 mm x 1 mm. Its shorter dimension is parallel to the transverse axis of the fiber. The flow rate of our gases is kept consistently at 45 ml/minute and 90 ml/minute for oxygen and hydrogen, respectively. We wish to maintain a 2:1 ration of hydrogen to oxygen in order to create a stable consistent flame. We also keep the flow rates low to ensure that the fiber is not being pushed outward by the gases as they exit the torch. The flame width can also be affected by the fact that our flame can reach temperatures beyond what is needed for pulling. If the flame is too hot then the effective flame width will appear to decrease. Having the fiber pull too quickly (due to high temperatures) can be detrimental as the shape may not be what the algorithm predicts and it can lead to deformations. Conversely, too large of an effective flame width can imply that the region of the flame the fiber is in is not hot enough, again leading to an improper shape. Fortunately, the torch is placed on a motorized stage (movement is perpendicular to the fiber) and is also attached to a two-dimensional translation stage. This enables us to move the torch three-dimensionally on a micron scale. As discussed above, since the flame has multiple heating zones, moving the torch will allow us to change the effective flame width. The method for measuring the flame width is the following. We set up a pulling with a constant fiber speed (usually 140 μm/s) and pull for two-second intervals. After each two-second interval, we measure the new diameter of the fiber waist using a microscope with a known resolution. We utilize equation (3.4) which describes the radius evolution (of the waist) for a given fiber speed, heating time and flame width. For this procedure, we set the torch speed to zero in order to simplify the radius evolution. By controlling the fiber speed and the duration the the pull, we can interpolate the effective flame

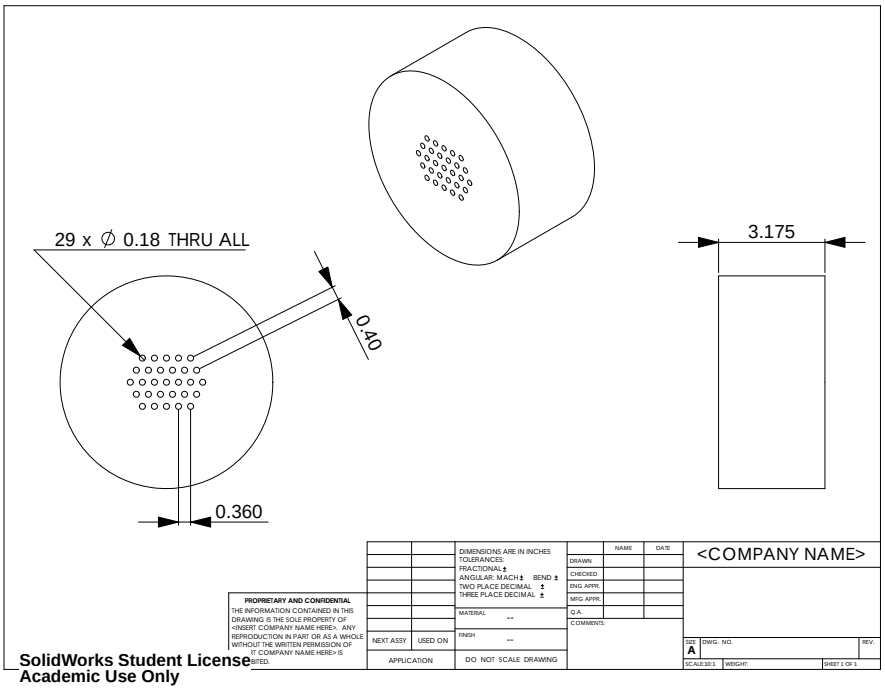

Figure 4.3: Design of the torch head. There are 29 holes in a hexagonal pattern, each with a diameter of 180 μm.

width. The measured diameters are plotted in a graph of $\ln\left(\frac{r_o}{r}\right)$ versus $\frac{tv_f}{2}$ which, according to (3.4), has a slope of L_o^{-1} (see figure 4.4). Thus, we can ascertain the effective flame width by performing a linear fit of this plot and taking the inverse of the resulting slope.

4.2.2 Pulling preparation

Upon knowing the effective flame width for our torch, we can proceed to calculate the fiber speeds and step times needed to produce a TNF of a desired geometry. This is done using a program which utilizes the equations and algorithm outlined in the previous chapter. The output is a list of speeds and times, for both motors, for every step. It is specially formatted to be read by our program which controls the motors. After running the simulation program, we examine the output; specifically, we look at the first step the motors have to execute and find the distance they must travel to complete the first step. This is important as the motors only have a finite range and, by default, begin at one

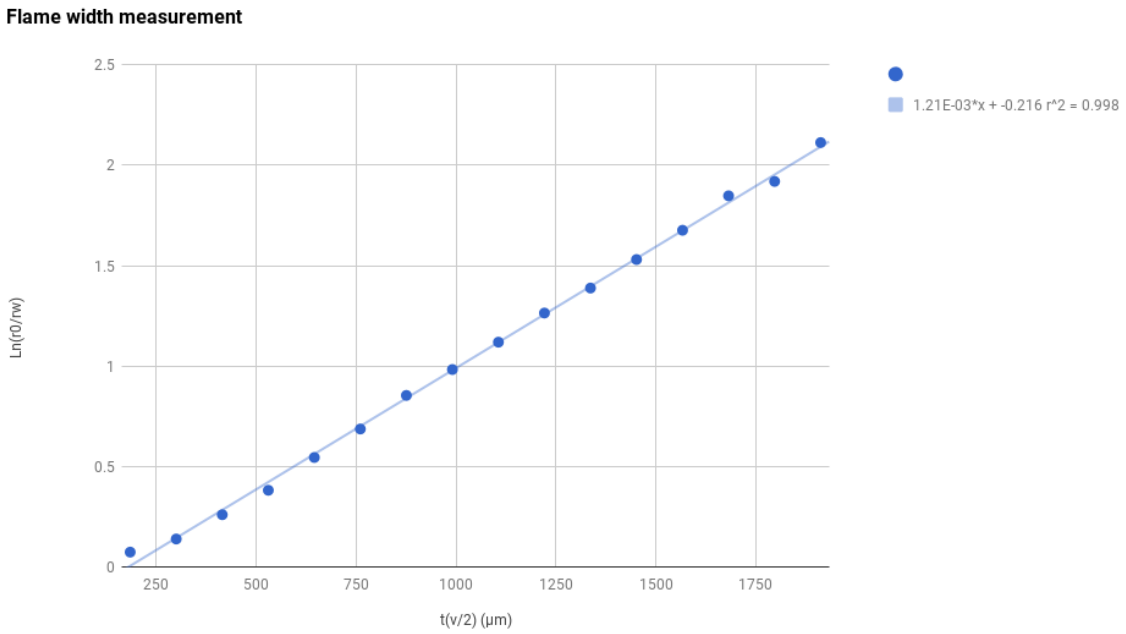

Figure 4.4: Example plot of a flame width measurement, the measured flame width was 826 μm. Each data point is separated by 2 seconds of pulling leading to a total pull time of 32 seconds. We use at least 30 seconds of pulling to ensure that we have a constant effective flame width (dictated by the linearity of the graph). The expected slope of the graph is L_0^{-1}.

end of their track. One motor has to be moved away from the other motor, such that this motor will not hit the end of its track before finishing the step. As a precaution, we do a test run of the pull (without a fiber) to ensure the motor has enough space.

4.2.3 Fiber preparation

Now, we can begin to prepare the fiber for pulling. All commercial optical fibers are coated with a plastic jacket to protect the fragile glass interior. However, this jacket is detrimental for pulling and a portion has to be removed before pulling. Furthermore, the jacket also prevents proper clamping of the fiber to the motorized stages. Adjusting the stages before this step allows us to know how much of the jacket needs to be stripped off. After stripping, we must clean the fiber thoroughly. Arguably the most significant part of preparation, the cleaning of the fiber has three steps. First, we use a Kimtech wipe with some acetone and gently wipe along the stripped portion of the fiber. This will clean off any remnants of the jacket left from the stripping. We follow this with isopropyl alcohol (IPA) on Kimtech wipes to remove anything that might have fallen onto the fiber after stripping and any pieces of the jacket remaining. Lastly, we use methanol on lens paper to clean anything that was missed in the previous steps. Finally, we use the microscope and scan across the length of the fiber to ensure that no contaminants remain. If any are found then the cleaning procedure is repeated from the beginning and the fiber is rechecked. When the fiber is deemed to be clean, it is properly placed in the clamps to ensure no slipping occurs during the pull. Apart from dust and contaminants, the other major detriment to pulling is over-tensioning or torsion. These can occur when clamping the fiber to the stage and can result in premature pulling when the fiber is first immersed in the flame. The result is often imperfections which lead to a loss in transmission or breakage of the fiber. To remedy this, the fiber is tensioned further by 200μm to guarantee over-tensioning and then detensioned by increments of 8μm. Both tensioning and detensioning are done by moving the stages away and toward each other, respectively. We view the fiber through the microscope and continue to detension the fiber until we can see a slight relaxation. Through the microscope, this looks like the fiber bowing downwards and then recovering back to its original

position. Upon seeing this, the fiber is deemed to be properly tensioned and pulling can begin.

4.2.4 Fiber extraction

The program will continue to move the motors until it runs out of speed and time values. At this point, the torch will be automatically disengaged and moved away from the fiber using its own motor. Now, if the transmission is acceptable ($> 95\%$), extraction of the fiber will begin. We start by tensioning the fiber very slightly in 4μm increments while monitoring the transmission; we stop if the transmission begins to decrease and detension one increment back to the optimum transmission. During pulling, the flowbox on top of the enclosure is turned off to prevent the flame from flickering. Once pulling is finished, the flowbox is turned back on to prevent dust from settling while the fiber is extracted. A C-shaped bracket is used to hold the taper in our vacuum chamber. After positioning the bracket such that the entire taper is enclosed, the fiber is glued to the bracket using vacuum-safe UV-curing glue. Finally, we place the fiber into our vacuum chamber and begin pumping down to ultra-high vacuum levels.

Chapter 5

Theory of TNF thermometry

5.1 General approach

We wish to have a nondestructive means of measuring the surface temperature of a TNF. Our approach is to use the phase shift of some probe beam, resulting from a change in the effective refractive index. This change of refractive index stems directly from an increase or decrease in TNF temperature. Thus, we first must establish a theory which enables us to ascertain the temperature from a shift in the phase of a probe beam. To do this, we will reproduce the theory first reported by Rauschenbeutel *et al.* [14]. Our goal is to fully demonstrate the theory such that any reader can readily calculate the temperature for their own experiments. We also need to adapt the original theory so that we can calculate the temperature from experimental phase measurements as opposed to using Bragg gratings like the original publication.

When a TNF is heated, it will experience both thermal expansion and a change in its refractive index. [14]. These factors alter the overall optical path length of the fiber which affect a propagating light beam in the form of a change it its phase. Given that the fiber is under tension in its mount, heating of the fiber will not result in any transverse lengthening, it will only reduce some of the stress that the fiber is experiencing. Therefore, we assume that there will be no physical length change of the fiber due to heating and only a radial expansion or refractive index change will occur. Thus, we can characterize this by some effective refractive index, n_{eff}, which is a function of both radius and the temperature dependent refractive index, $n(T)$. The formula for n_{eff} is given by

$$\frac{\partial n_{\text{eff}}(a,T)}{\partial T} = \frac{\partial n_{\text{eff}}(a,T)}{\partial n}\left(\frac{\partial n(T)}{\partial T} - n\alpha_{te}\alpha_{so}\right) + \frac{\partial n_{\text{eff}}(a,T)}{\partial a}(1+\mu_P)\,\alpha_{te}a \tag{5.1}$$

where α_{te} is the thermal expansion coefficient for silica which is in the range of $(4-7)\times 10^{-7}K^{-1}$. $\alpha_{so} = -0.206$ and $\mu_P = -0.168$ are the strain-optic coefficient and the Poisson's ratio for silica.

a is the radius of the TNF. $\frac{\partial n(T)}{\partial T}$ is the thermo-optic coefficient for silica, which was empirically found by Rauschenbeutel *et al.* to be [14],

$$\frac{\partial n(T)}{\partial T} = 9.627(9) \times 10^{-6} + 7.74(1) \times 10^{-9}(T - 299K) \tag{5.2}$$

Now, we can integrate eq. (5.1) to obtain the effective refractive index which enables us to calculate the change in the optical path length. The total change in the optical path length (which is not the same as the physical length) is the change of the effective refractive index (due to temperature and radial changes) integrated over the length of the fiber.

$$\Delta l = \int_{-l_0/2}^{l_0/2} [n_{\text{eff}}(a(z), T(z)) - n_{\text{eff}}(a(z), T_0)]\, dz \tag{5.3}$$

z is chosen to be along the transverse axis of the fiber. Finally, we can get the phase accumulation by

$$\Delta\phi = \frac{2\pi\Delta l}{\lambda} \tag{5.4}$$

The radial function, $a(z)$, is obtained during our theoretical simulation of our fiber pulling. However, the temperature profile, $T(z)$, can only be obtained by understanding the thermodynamics of optically heating a fiber. We will now present the theory of the thermodynamics of TNFs.

5.2 Fluctuational Electrodynamics (FED) Calculations

It was shown by Rauschenbeutel *et al.* that the heat radiation of the nanofiber is not accurately modeled by Planck's or Stefan-Boltzmann's laws [14]. Both of these theories are accurately applied to far-field heat radiation of macroscopic objects. However, when the object reaches dimensions below the thermal wavelength, near-field effects like diffraction and wave interference and tunneling become significant [15]. Objects with such small dimensions are expected to considerably deviate from the Stefan-Boltzmann radiation law. This deviation occurs when the size of the object is comparable to the emitted wavelength. Interference effects can modify the spectral power density

of radiation, enhancing emission at certain wavelengths[10]. Consequently the radiated heat must be evaluated from first principles using fluctuational electrodynamics (FED) [16]. Macroscopic theories will no longer hold in this regime and, thus, we must apply a model such as FED to the fiber. We begin with an equation describing the total thermodynamical effects.

$$\begin{aligned} c_p \rho \partial_t T = &-\frac{dH_{\text{rad}}(T)}{dV} + \frac{dH_{\text{rad}}(T_0)}{dV} + \nabla(\lambda_c \nabla T) \\ &+\frac{dP_{\text{heating}}}{dV} - \sqrt{\frac{k_B f^2}{8\pi M T_0}} p(T - T_0)\frac{dS}{dV} \end{aligned} \tag{5.5}$$

where c_p is the specific heat capacity, ρ is the density, λ_c is the heat conductivity, T is the fiber temperature and T_0 the room temperature. ∂_t represents a partial derivative with respect to time. The first two terms on the right-hand side of the equation describe the heat exchange by radiation. dP_{heating} is the source of heat, namely the the heat generated by the light coupled into the fiber. k_B is Boltzmann's constant, f and M are the degrees of freedom and molecular mass of the environment gas (usually taken to be diatomic nitrogen), T_0 is room temperature, p is the pressure of the gas and S is the surface area. The last term, depending on background pressure of the environment, can safely by neglected as the fiber is under ultra high vacuum ($p \approx 10^{-8}$ Torr).

To solve Eq. (5.5) we neglect temperature variations over a cross section of the fiber considering only its variation along the fiber axial coordinate z. Consequently Eq. (5.5) can be written as:

$$\begin{aligned} c_p \rho \partial_t T \pi a(z)^2 = &-\partial_z H_{rad}(T) + \partial_z H_{rad}(T_0) \\ &+\lambda_c(\partial_z^2 T)\pi a(z)^2 + \partial_z P_{\text{heating}} \end{aligned} \tag{5.6}$$

where T is a function of z and t, $a(z)$ is the z dependent fiber radius profile.

The following is a model calculating the heat radiation of a cylinder reproduced from [17]. Along the transverse axis of an infinite cylinder, of some isotropic material, with radius a at some tem-

perature T_c, the heat radiated per unit length is represented as

$$\begin{aligned}\partial_z H_{rad} = \frac{4}{c_0}\int_0^\infty d\nu \frac{h\nu^2}{exp(h\nu/k_B T_c)-1} \sum_{P=\perp,\parallel}\sum_{l=-\infty}^{\infty} \\ \times \int_{-1}^{1} d\xi (Re(T_{l,\xi}^{PP}) + |T_{l,\xi}^{PP}|^2 + |T_{l,\xi}^{P\overline{P}}|^2)\end{aligned} \tag{5.7}$$

where c_0 is the speed of light in vacuum, ν is the optical frequency, P is the polarization of the radiated light with respect to the plane of propagation, l is the mode number and $\overline{P}$ denotes the perpendicular polarization to P. $\xi := \frac{k_z}{k_0}$, where $k_0 = 2\pi\nu/c_0$, is the ratio between the axial (k_z) and vacuum (k_0) propagation constants. The matrix elements, $T_{l,\xi}^{PP'}$, of the $\mathbb{T}$ operator represent the response of the amplitude of a scattered electromagnetic wave with polarization P to an incoming wave with polarization P' [17]. For a cylinder, these elements are written as

$$\begin{aligned} T_{l,\xi}^{\perp\perp} &= -\frac{J_l(qa)}{H_l^{(1)}(qa)}\frac{\Delta_1\Delta_4 - K^2}{\Delta_1\Delta_2 - K^2}, \\ T_{l,\xi}^{\parallel\parallel} &= -\frac{J_l(qa)}{H_l^{(1)}(qa)}\frac{\Delta_2\Delta_3 - K^2}{\Delta_1\Delta_2 - K^2}, \\ T_{l,\xi}^{\perp\parallel} = T_{l,\xi}^{\parallel\perp} &= -\frac{2iK}{\pi\sqrt{\varepsilon\mu}(qaH_l^{(1)}(qa))^2}\frac{1}{\Delta_1\Delta_2 - K^2}, \end{aligned} \tag{5.8}$$

where

$$\begin{aligned} \Delta_1 &= \frac{J_l'(q_1a)}{q_1aJ_l(q_1a)} - \frac{1}{\varepsilon}\frac{H_l^{(1)\prime}(qa)}{qaH_l^{(1)}(qa)}, \\ \Delta_2 &= \frac{J_l'(q_1a)}{q_1aJ_l(q_1a)} - \frac{1}{\mu}\frac{H_l^{(1)\prime}(qa)}{qaH_l^{(1)}(qa)}, \\ \Delta_3 &= \frac{J_l'(q_1a)}{q_1aJ_l(q_1a)} - \frac{1}{\varepsilon}\frac{J_l'(qa)}{qaJ_l(qa)}, \\ \Delta_4 &= \frac{J_l'(q_1a)}{q_1aJ_l(q_1a)} - \frac{1}{\mu}\frac{J_l'(qa)}{qaJ_l(qa)}, \\ K &= \frac{l\xi k_0 c_0}{\sqrt{\varepsilon\mu}a^2\omega}(\frac{1}{q_1^2} - \frac{1}{q^2}), \\ q &= k_0\sqrt{1-\xi^2}, \text{ and} \\ q_1 &= k_0\sqrt{\varepsilon\mu - \xi^2} \end{aligned} \tag{5.9}$$

$J_l(x)$ is the Bessel function of the first kind, $H_l^{(1)}(x)$ is the Hankel function of the first kind and

prime indicates a derivative such that $f'(x) = \partial_x f(x)$. ε and μ represent the relative permittivity and permeability of silica.

5.3 Heating Power

The source term in Eq. (5.6) is $\partial_z P_{\text{heating}}$ which denotes the heat absorbed per unit length. Its evaluation is based on the assumption that the fiber heating is essentially due to energy absorption and dissipation occurring at the surface of the fiber, predominantly due to surface pollutants [13]. A constant surface density of absorbers on the fiber surface is assumed. In consequence $\partial_z P_{\text{heating}}$ can be written as:

$$\partial_z P_{\text{heating}} = k 2\pi a(z) I(a(z))\, dz \tag{5.10}$$

where $I(a(z))$ is the position-dependent intensity profile of the propagated light mode in cylindrical coordinates. k is a proportionality constant that depends the surface density of absorbers and the scattering cross section. This is the only fit parameter and it is adjusted such that the resulting phase accumulation from theory will match what is observed in the experiment. Once an appropriate value for k is found, we verify that all experimental data agrees with theory.

From here, we must determine the surface intensity profile for the fiber. This can be done via the Poynting vector, S, which is obtained by examining the electric and magnetic fields propagating through the fiber. The equations for these fields were presented in chapter 2, and we can obtain the Poynting vector with,

$$I(a(z)) = |A(P_0)|^2 S_z(a(z)) = |A(P_0)|^2 \left(E_r(a(z)) H_\theta(a(z)) - E_\theta(a(z)) H_r(a(z))\right) \tag{5.11}$$

where $E_{r,\theta}(a(z))$ and $H_{r,\theta}(a(z))$ are the cylindrical components of the electromagnetic fields propagating through the fiber (discussed in chapter 2). $A(P_0)$ is a global constant which depends on the input optical power P_0. $A(P_0)$ is found by integrating the intensity across the the surface area of the fiber; this is equal to the input power (assuming no loss). Note that $S_r = S_\theta = 0$ which coincides with the fact that the light should only propagate along the fiber, excluding any scattering by con-

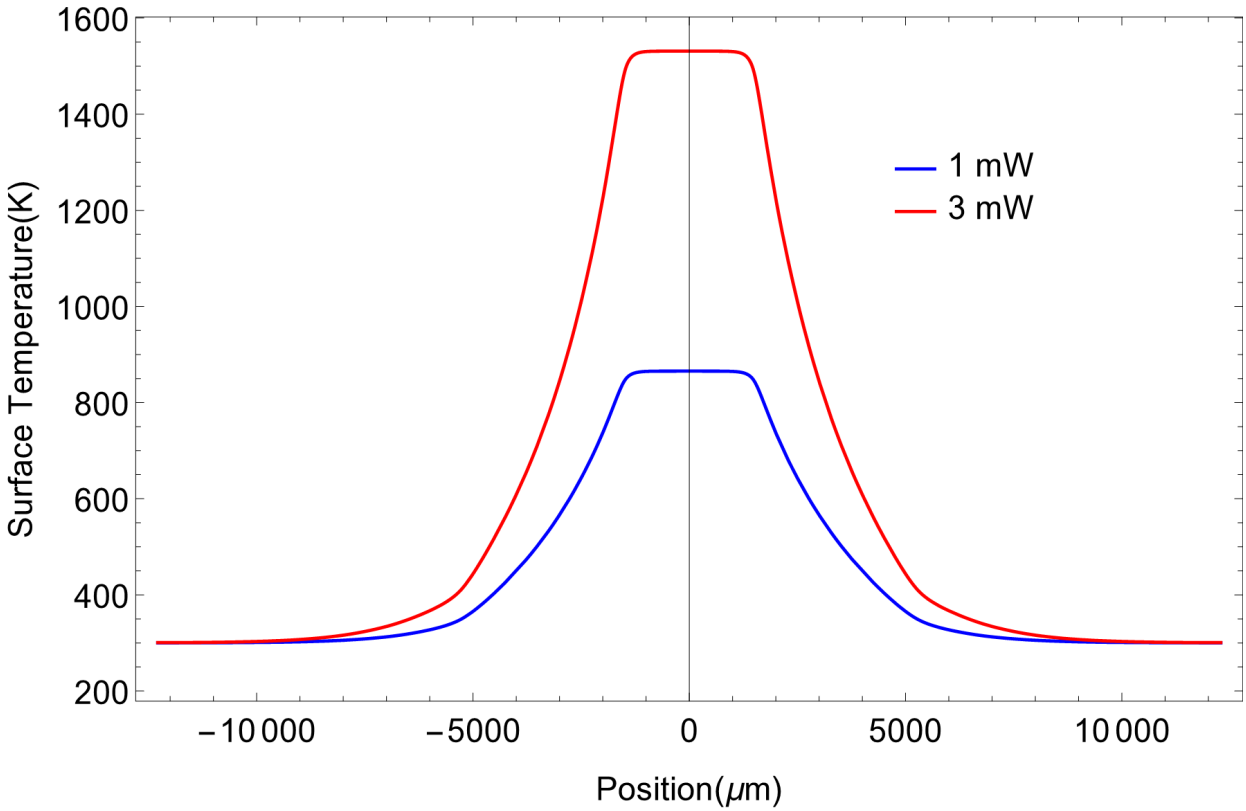

Figure 5.1: Theoretical temperature profile of the fiber at equilibrium. Graph plotted for input optical power of 1 mW and 3 mW. The proportionality constant $k = 0.0306$ for both powers. The position 0 is denoted as the center of the fiber.

taminants. Finally, we can numerically solve (5.6) to obtain the temperature profile, $T(a(z))$ which can then be used in (5.3) to get the path length change and, therefore, the phase accumulated by the beam.

An example plot of the radius-dependent surface temperature is shown if fig. 5.1. We use the fiber radius profile generated by our pulling algorithm to plot the temperature as a function of position on the fiber instead of radius. One can see that the temperature is large at the fiber waist (between -2500 μm and 2500 μm) and decreases significantly along the tapered region. The temperature returns to ambient levels (300 K) 1 cm beyond the center.

Chapter 6

Experimental thermometry of optical nanofibers via double heterodyne detection

6.1 Experiment

TNFs with very high transmissions ($> 98\%$) can now be made with relative ease, and can withstand very high optical powers propagating through them (10-100mW). However, the small size and high evanescent intensity makes the nanofibers extremely fragile. Though the absorption in the fiber glass is normally negligible, any dissipation due to imperfections or contamination of the fiber surface results in heating that can easily provoke the destruction of the nanofiber. It is therefore important to have a means of monitoring the temperature of the nanofiber in the region of its waist. Also, since interaction with atoms is required and leads to possible adsorption, a controlled heating of the nanofiber can be useful for the desorption of contaminants from the fiber surface.

The methods suggested for nanofiber temperature monitoring rely on the temperature dependent variation of the refractive index of the fiber material (silica). This variation results in the modification of the optical path-length and, consequently, the phase of the transmitted optical field. The first study of nanofiber heating was presented in [14]. The optical fiber used in that work had Bragg reflecting gratings built at both ends of the fiber thus realizing an optical cavity. Variations of the optical phase resulted in changes of the transmission through the cavity and gave access to the temperature dependent changes of the refractive index. However, many experiments utilizing nanofibers do not require Bragg gratings. Thus, adding one or manufacturing a nanofiber from a commercial Bragg-grating optical fiber would prove arduous if only for the sake of temperature monitoring.

In this thesis we demonstrate an alternate method for nanofiber temperature monitoring. Our method exploits the phase sensitivity of balanced optical heterodyne detection [18] and can readily be implemented with any single mode fiber without the need of Bragg reflectors at the fiber ends. The principle of the method is as follows: a weak light field is sent along the fiber. The output light is combined in a beam splitter (BS) with a local oscillator (LO) light beam whose frequency is shifted by Δ with respect to the probe field. The two beams after the BS are sent to identical fast photodetectors and the corresponding photocurrents are subtracted. This constitutes the usual optical balanced heterodyne detection (BHD) setup. As a result of the frequency shift between the signal and the LO, the BHD output is modulated at the frequency Δ. A change in the signal phase results in the same change in the phase of the modulated BHD output.

The choice of the frequency Δ is usually guided by practical considerations. Most of the technical noise in lasers occurs at frequencies below a few MHz. It is thus customary to perform BHD with frequencies larger than several MHz [19]. In our case we have used $\Delta = 130$MHz. For this frequency, the BHD is shot-noise limited allowing a very good phase sensitivity [19]. However, the time domain analysis of the signal over a total time range of several seconds would require large data storage amounts and very fast data acquisition (DAQ) equipment. To circumvent this difficulty, we have down-shifted the oscillation frequency by performing a second heterodyne mixing of the modulated output of the BHD with a RF signal at frequency $\Delta + \delta$ with $\delta = 20$kHz. After passage through a low-pass filter (cut-off frequency $\sim$ 1 MHz) the mixer output has a modulation of 20 kHz. The reduced frequency signal is recorded in a digital oscilloscope and its phase variations are monitored with respect to a 20 kHz reference.

The experimental setup is shown in Fig. 6.1. We used a tapered nanofiber produced, from a commercial single-mode optic fiber, using an oxy-hydrogen flame and a flame-brush technique (see chapter 4). During the experiment the tapered portion of the fiber was inside a vacuum chamber designed for Rb magneto-optical cooling. A 795 nm Titanium Sapphire "heating" laser is coupled

into the nanofiber with a power ranging from 250 μW to 5 mW. A portion of this power is absorbed by the fiber which results in heating. A very weak ($< 10\mu$W) 780 nm probe beam is also coupled into the fiber; the change in refractive index will induce a phase shift of the probe. Once exited from the fiber, the probe beam is mixed with a strong LO, originating from the same laser, and sent to the BHD setup. The probe beam is frequency shifted with respect to the LO with an acousto-optic modulator (AOM) driven by an RF wave of 130 MHz. To down-shift the BHD signal to 20 KHz, this signal is mixed with a second RF wave of 130.02 MHz and low-pass filtered. A 20 kHz phase reference signal is also generated by the mixing of two mentioned RF waves. All RF waves are generated by the same direct digital synthesizer (DDS). The choice of the 20 KHz frequency is dependent on the rate of the phase change of the probe beam. With this choice, the induced change in the probe beam phase over one period is always smaller than 2π.

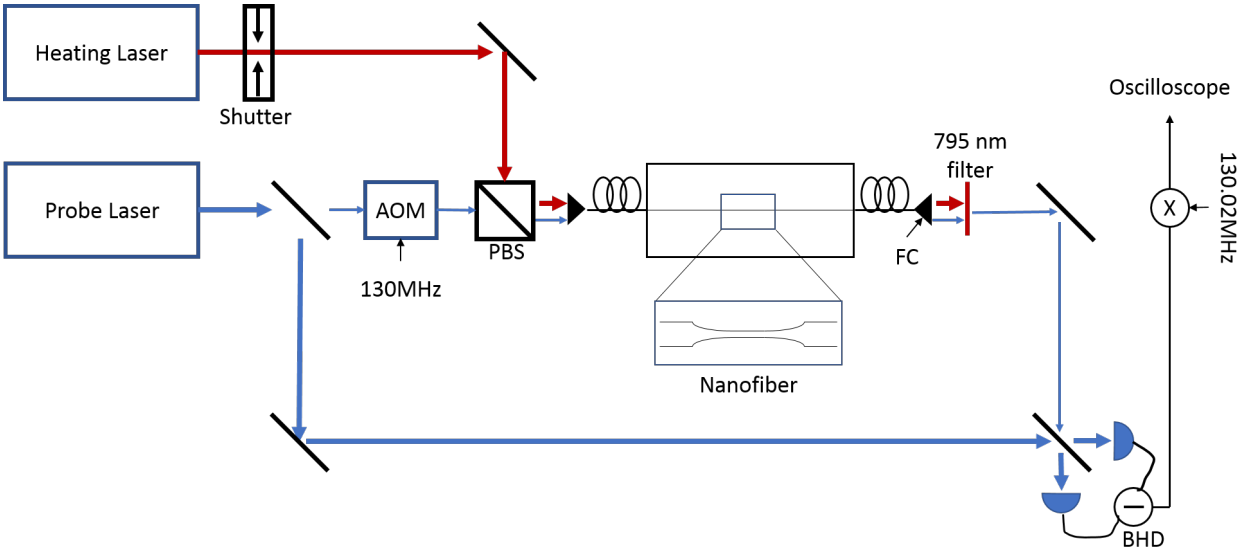

Figure 6.1: Experimental setup. Abbreviations: PBS(Polarized Beam Splitter), FC (Fiber Coupler), BHD (Optical Balanced Heterodyne Detector), AOM (Acousto-Optic Modulator). The nanofiber is housed in a vacuum chamber under ultra-high vacuum ($\leq 10^{-8}$ Torr.

A mechanical shutter placed on the path of the heating laser was used to create successive heating and cooling cycles of 2 seconds duration; longer cycles produced no significant phase change. The measured accumulated phase variation during heating and cooling are presented in Fig. 6.2. When the shutter is open and the fiber is being heated, we see a very fast increase in phase until an

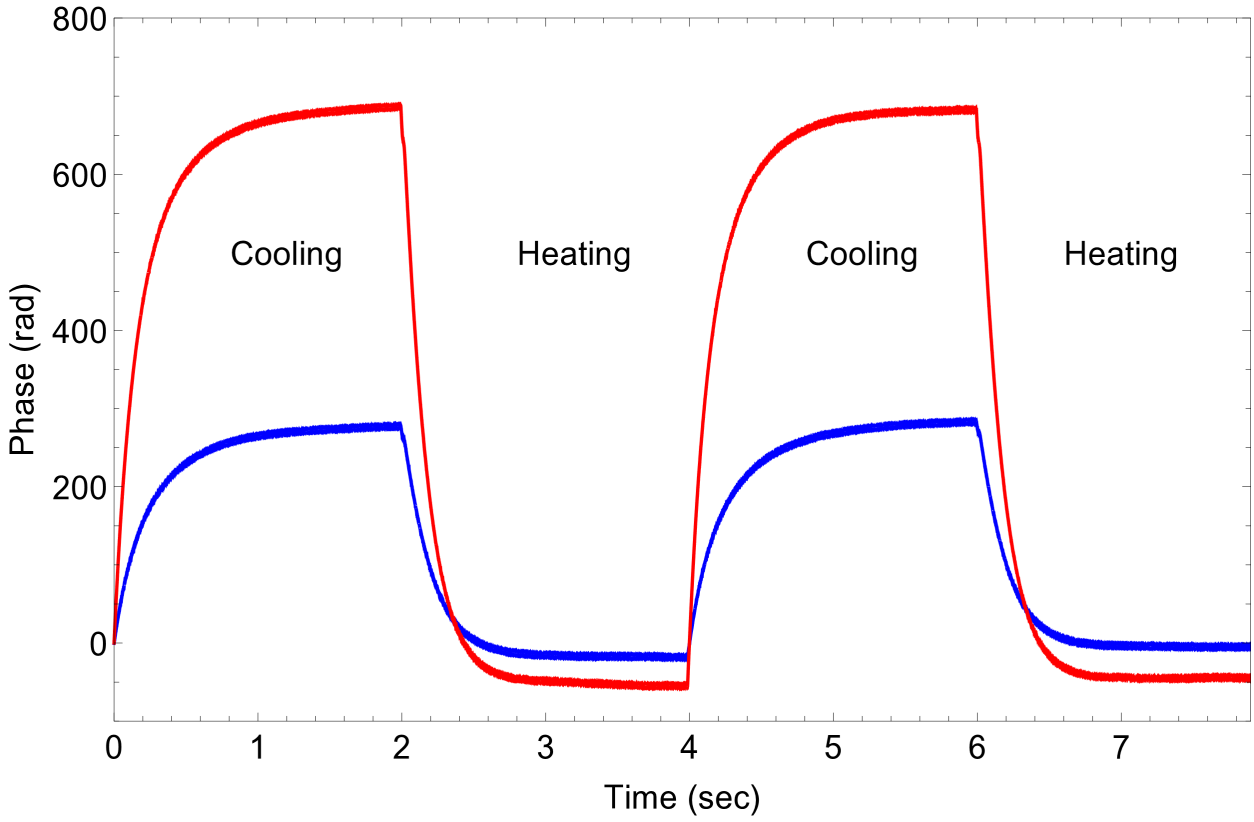

Figure 6.2: Phase accumulated for heating and cooling cycles for transmitted power of 1 mW (blue) and 3 mW (red).

equilibrium is reached. Once the shutter is closed, we see a very fast decrease in phase to the original level and then an equilibrium is again reached. This behaviour conforms well with a typical thermodynamical response of an object being heated and cooled. We take the change in phase due to heating, at equilibrium, and plot it as a function of the input optical power of the heating laser in fig. 6.3. The blue region in the figure displays the predicted theoretical phase change including uncertainties; the greatest uncertainty being the radius (5%). The fiber used in this experiment had a waist radius of 230 nm and a waist length of 5 mm. From here, we utilized the theory outlined in chapter 5 to ascertain the surface temperature of the fiber waist that corresponds to the experimental phase measurements. These temperatures are shown in fig. 6.4 and correspond to the phase data shown in fig. 6.3 for the same input power.

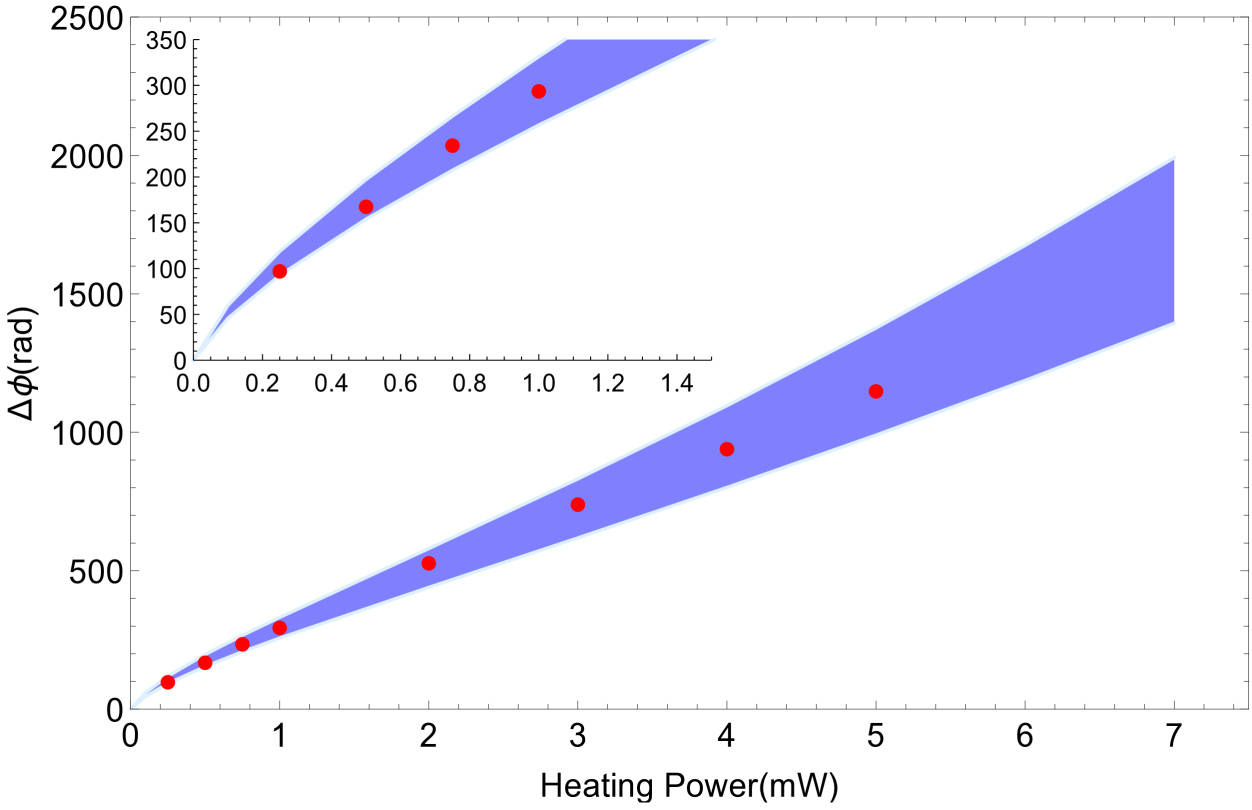

Figure 6.3: Phase difference between heating and cooling cycles as a function of heating power.The experimental data(red points) is within the predicted errors(blue) even for low heating powers(inset). The primary source of error is the uncertainty(5%) in the radius profile of the nanofiber.

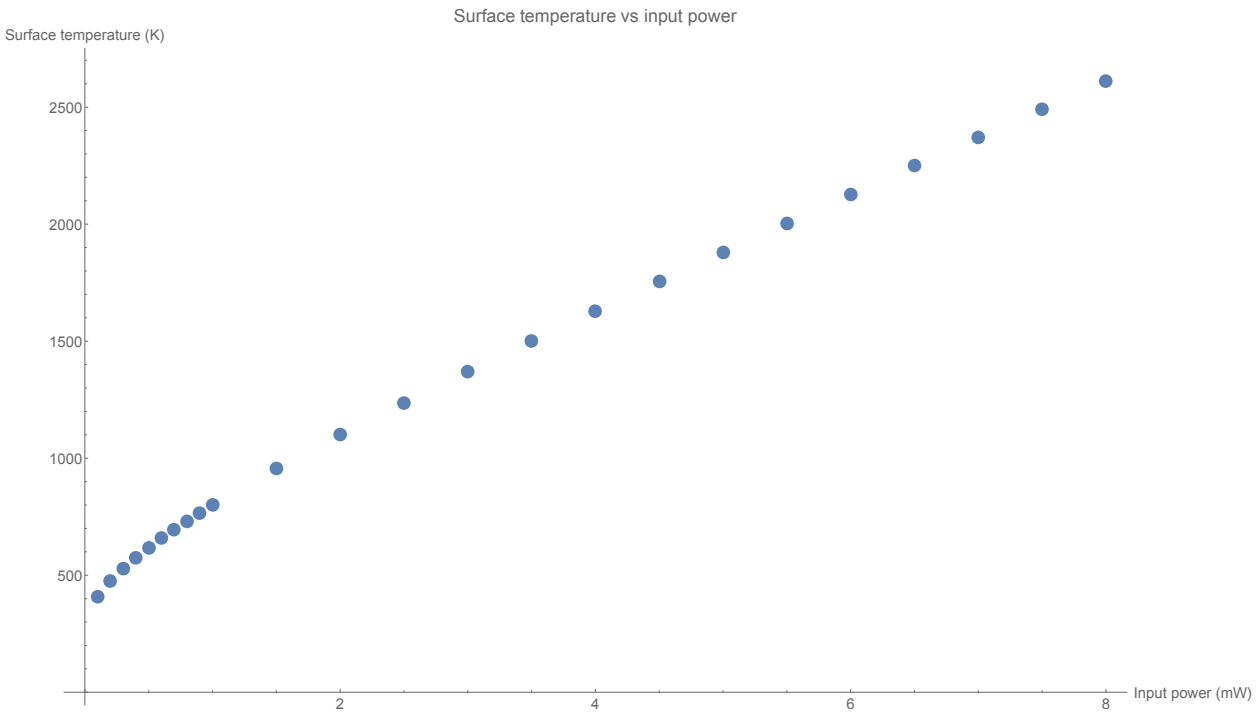

Figure 6.4: Surface temperature at the waist of the nanofiber as a function of input power. These temperatures correspond to the phase data displayed in fig. 6.3 for the same input power.

6.2 Rubidium desorption

Our experimental apparatus is intended for the efficient coupling of magneto-optically cooled ^{87}Rb atoms with the evanescent optical field surrounding the nanofiber. One challenge faced by our systems is the accumulation of atoms on the surface of the fiber [13]. As atoms adsorb onto the fiber, its transmission decreases due to the scattering of the coupled light [13]. This is not only detrimental to the light transmission, but also to the structural stability of the fiber as well since the scattered light leads to localized heating. A solution to this problem consist in controllably heating the fiber, enough to desorb the atoms, without structurally damaging it.

Pittman *et al.* investigated the possibility of recovering, and preserving, the transmission of a nanofiber in rubidium vapor [20]. Their method utilized an external heater mounted onto the fiber holder to control the surface temperature of the fiber. This enabled them to recover a portion of the lost transmission and preserve a fiber's transmission with some success. However, they did not report the complete recovery of a fiber's transmission after degradation. Also, their external heat-

ing apparatus considerably reduces the access to the nanofiber environment. Suggestions have also been made about the possibility of using light-induced atomic desorption (LIAD). LIAD involves the use of ultraviolet light to cause desorption via the heating of the glass or coating on the glass [21]. However, the use of an external light source proved to be not useful. Based on our observations while attempting to use LIAD using an external LED curing lamp (using a wavelength range of 475 nm - 495 nm and an intensity range of 5 mW/cm^2 and 20 mW/cm^2), there appears to be no significant desorption from the fiber surface. This could be due to the fact that the fiber is enclosed in a vacuum chamber and the light must pass through glass windows before reaching the fiber. In principle, if the fiber were to heat up via absorption then a significant portion of the light would be absorbed by the glass windows. Another possibility is that the absorption of ultraviolet light in glass is simply too small to create enough heat. Based on past literature of LIAD experiments, most involve a coating on glass which is the focus of the experiment which could imply a lack of absorption in bare glass.

Making use of our ability to precisely monitor the nanofiber temperature, we have studied the desorption of Rb atoms from the fiber surface resulting from the heat provided by an external laser transmitted through the fiber. Initially a cold atomic cloud of ^{87}Rb is formed in a magneto-optical trap (MOT) in the proximity of the nanofiber. After overlapping the rubidium cloud with the fiber we observed a significant drop (more than 80%) in the transmission through the fiber (see figure 6.5). In addition to a weak power probe laser, used to monitor the fiber transmission, a variable-power laser is used for heating. The initial power of the heating laser was 25 μW and was then slowly increased, in 25 μW increments, until we saw a noticeable change in the probe beam power. We continued to increase the power of the heating laser, while monitoring the fiber transmission, until we no longer observed an increase in transmission. The results of this experiment are reported in fig. 6.5. A recovery of the fiber transmission to near 90% of the original value is observed. Although this is not a full recovery of the transmission, we believe it is the most significant recovery of transmission compared to other reports involving TNFs.

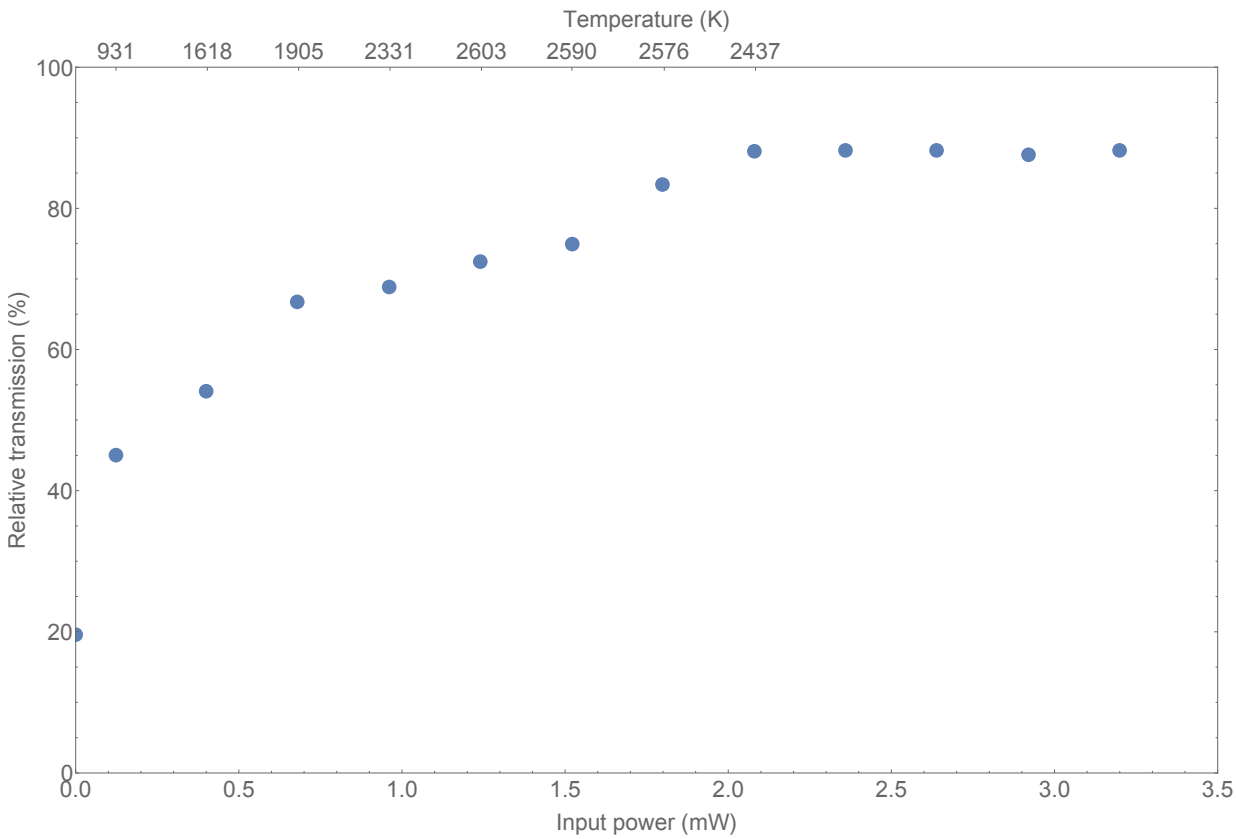

Figure 6.5: Relative transmission of the fiber and the corresponding surface temperature (purple) as a function of the transmitted heating power (blue).

The temperatures associated with the transmissions are also reported in fig. 6.5. We note a steady increase in the required temperature to increase the transmission until the fiber had recovered approximately 65% of its original transmission. We believe this is due to the fact that the temperature results from two factors. One is the input power and the other is the amount of adsorbed contaminants on the surface. Since the amount of adsorbers is inversely proportional to the transmission, it is understandable that there will be a point where a max temperature is reached. After this there is a decrease in temperature which appears to be correlated to an increase in transmission. We believe that the temperature will begin to increase again as input power is increased by transmission remains constant.

Chapter 7

Conclusion and outlook

Presented in this thesis is the successful synthesis and characterization of low-loss tapered nanofibers for use in quantum optics experiments. The synthesis was achieved by upgrading our pulling setup as well as utilizing an algorithmic approach to programmatically pull fibers. We further improved our understanding of these nanofibers by studying their thermodynamics, in the hope that we can avoid fiber breakage and recover lost transmission. These improvements will enable our group to continue progressing towards more advanced experiments in quantum information processing (QIP) with the aid of TNFs.

We achieved the latter objectives using the following. We established the necessary calculations for the fields propagating through a nanofiber. This includes the calculation of the propagation constant β and the electromagnetic fields for both inside and outside the fiber, for the optical frequencies that pertain to our research. This allows us to know what geometries (i.e. waist diameter and waist length) are optimal for our particular experiments. We then needed to have a means of manufacturing such a fiber consistently and reliably with low loss. To do this, we theoretically studied the evolution of a fiber's profile as it is pulled by a constant heat source. From this, we constructed an algorithm which uses the knowledge of the profile evolution to iteratively adjust the step-by-step pulling speeds and durations to obtain the desired nanofiber. We sought to develop our own program as other groups have either not made their program publicly available or there are some errors which exist that prevent us from simulating the fibers that we wish to create. Subsequently, we produced an experimental procedure to complement our algorithm. We built a dust-free enclosure to encase our pulling rig and composed a protocol for cleaning the fiber beforehand along with preparing the rig to pull a specific fiber properly.

Next, we detailed an experiment designed to probe the thermodynamics of a TNF. We analyzed

the theory behind the thermodynamics of a sub-thermal wavelength object and discovered a way to calculate the nanofiber's surface temperature as a function of radius and input optical power. This enables us, when experimentally measuring phase shifts experienced by a weak probe laser traveling through the nanofiber, to infer the temperature of the TNF. Afterwards, we reported an experiment which measured the aforementioned phase shifts using double heterodyne measurements and discovered the trend of temperature as a function of input power. Additionally, we hypothesized the concept of using a laser field, propagating through the TNF, to heat a fiber contaminated by adsorbed atoms enough to desorb these atoms and recover any lost transmission. This hypothesis proved plausible as we managed to recover almost 90% of transmission, that was lost due to purposeful contamination of the fiber by atoms, by controllably heating of the nanofiber using a laser field.

Based on the results reported in this thesis, the outlook of these fiber experiments appear to be quite promising. The success of creating custom low-loss nanofibers, coupled with the successful transmission recovery of a nanofiber, creates many possibilities for this research. The ability to send strong laser fields through the fiber, without fear of breakage, allows for experiments involving dipole traps. These dipole traps allow the trapping of many atoms very close to the fiber, increasing the optical depth for quantum optics experiments. Such an increase has been demonstrated in the past by Kimble's group in 2012 [22]. This implies that our group could push further, significantly, to perform experiments which are very meaningful to the field of quantum information processing. These experiments include the realization of cross phase modulation (XPM) [23] or the Duan, Lukin, Cirac, and Zoller (DLCZ) [24] protocol using TNFs. Currently, our hopes would be to improve on past experiments with TNFs, such as the realization electromagnetic-induced transparency in free space [25]. In essence, our desire, and possible plan moving forward, is to perform many critical QIP experiments with nanofibers. Such experiments, which have been previously demonstrated in free space, could be greatly enhanced using TNFs towards the realization of a physical implementation for quantum information processing.

Bibliography

[1] Pieter Kok, W. J. Munro, Kae Nemoto, T. C. Ralph, Jonathan P. Dowling, and G. J. Milburn. Linear optical quantum computing with photonic qubits. *Rev. Mod. Phys.*, 79:135–174, Jan 2007.

[2] F. De Martini, G. Innocenti, G. R. Jacobovitz, and P. Mataloni. Anomalous spontaneous emission time in a microscopic optical cavity. *Phys. Rev. Lett.*, 59:2955–2958, Dec 1987.

[3] Hashem Zoubi and Helmut Ritsch. Hybrid quantum system of a nanofiber mode coupled to two chains of optically trapped atoms. *New J. Phys.*, 12(10):103014, 2010.

[4] J. M. Ward, A. Maimaiti, Vu H. Le, and S. Nic Chormaic. Contributed review: Optical micro- and nanofiber pulling rig. *Rev. Sci. Instrum.*, 85(11):111501, 2014.

[5] J. C. Knight, G. Cheung, F. Jacques, and T. A. Birks. Phase-matched excitation of whispering-gallery-mode resonances by a fiber taper. *Opt. Lett.*, 22(15):1129–1131, Aug 1997.

[6] TAKANORI OKOSHI. 4 - wave theory of uniform-core fibers. In TAKANORI OKOSHI, editor, *Optical Fibers*, pages 48 – 81. Academic Press, 1982.

[7] V. I. Balykin, K. Hakuta, Fam Le Kien, J. Q. Liang, and M. Morinaga. Atom trapping and guiding with a subwavelength-diameter optical fiber. *Phys. Rev. A*, 70:011401, Jul 2004.

[8] K. Karapetyan. *Single optical microfibre-based modal interferometer.* PhD thesis, Rheinische FriedrichWilhelms-Universität Bonn, 2012.

[9] T. A. Birks and Y. W. Li. The shape of fiber tapers. *J. Lightwave Technol.*, 10(4):432–438, Apr 1992.

[10] C. Wuttke. *Thermal excitations of optical nanofibers measured with a fiber-integrated Fabry-Pérot cavity.* PhD thesis, Johannes Gutenberg Unversität Mainz, 2014.

[11] J. E. Hoffman, S. Ravets, J. A. Grover, P. Solano, P. R. Kordell, J. D. Wong-Campos, L. A. Orozco, and S. L. Rolston. Ultrahigh transmission optical nanofibers. *AIP Adv.*, 4(6):067124, 2014.

[12] Ryutaro Nagai and Takao Aoki. Ultra-low-loss tapered optical fibers with minimal lengths. *Opt. Express*, 22(23):28427–28436, Nov 2014.

[13] Masazumi Fujiwara, Kiyota Toubaru, and Shigeki Takeuchi. Optical transmittance degradation in tapered fibers. *Opt. Express*, 19(9):8596–8601, Apr 2011.

[14] C. Wuttke and A. Rauschenbeutel. Thermalization via heat radiation of an individual object thinner than the thermal wavelength. *Phys. Rev. Lett.*, 111:024301, Jul 2013.

[15] Y. Zheng. Review of fluctuational electrodynamics and its applications to radiative momentum, energy and entropy transport. *ArXiv e-prints*, October 2014.

[16] Karl Joulain, Jean-Philippe Mulet, Franois Marquier, Rmi Carminati, and Jean-Jacques Greffet. Surface electromagnetic waves thermally excited: Radiative heat transfer, coherence properties and casimir forces revisited in the near field. *Surf. Sci. Rep.*, 57(34):59 – 112, 2005.

[17] Vladyslav A. Golyk, Matthias Krüger, and Mehran Kardar. Heat radiation from long cylindrical objects. *Phys. Rev. E*, 85:046603, Apr 2012.

[18] P. Beaud, J. Schutz, W. Hodel, H. P. Weber, H. H. Gilgen, and R. P. Salathe. Optical reflectometry with micrometer resolution for the investigation of integrated optical devices. *IEEE J. Quantum Electron.*, 25(4):755–759, Apr 1989.

[19] A. I. Lvovsky. *Squeezed Light*, pages 121–163. John Wiley and Sons, Inc., 2015.

[20] Meimei Lai, James D. Franson, and Todd B. Pittman. Transmission degradation and preservation for tapered optical fibers in rubidium vapor. *Appl. Opt.*, 52(12):2595–2601, Apr 2013.

[21] A. Burchianti, C. Marinelli, A. Bogi, E. Mariotti, V. Biancalana, S. Veronesi, and L. Moi. Light induced desorption and diffusion of alkali atoms in porous glasses. In *EQEC '05. European Quantum Electronics Conference, 2005.*, pages 217–, June 2005.

[22] A. Goban, K. S. Choi, D. J. Alton, D. Ding, C. Lacroûte, M. Pototschnig, T. Thiele, N. P. Stern, and H. J. Kimble. Demonstration of a state-insensitive, compensated nanofiber trap. *Phys. Rev. Lett.*, 109:033603, Jul 2012.

[23] H. Schmidt and A. Imamoglu. Giant kerr nonlinearities obtained by electromagnetically induced transparency. *Opt. Lett.*, 21(23):1936–1938, Dec 1996.

[24] L.-M. Duan, M. D. Lukin, J. I. Cirac, and P. Zoller. Long-distance quantum communication with atomic ensembles and linear optics. *Nature*, 414:413 EP –, Nov 2001. Article.

[25] A. MacRae, G. Campbell, A. Ordog, and A. I. Lvovsky. Simultaneous Slow Light Pulses With Matched Group Velocities via Double-EIT. In A. Lvovsky, editor, *American Institute of Physics Conference Series*, volume 1110 of *American Institute of Physics Conference Series*, pages 269–272, April 2009.